AUTOMATED GENERATION OF GLOBAL CLOUD DATASETS FROM POLAR ORBITING SATELLITES. PART I: CLAVR-2 PIXEL-SCALE MULTIPLE LAYER CLOUD ANALYSES (MLCA)

P A. Davis[1], L. L. Stowe[2], G. Luo[3], E. P. McClain[4], A. K. Heidinger[2]

ABSTRACT

Development of the CLAVR-2 (CLouds from AVHRR - Phase 2) algorithm completes the evolution of a system, applicable in real time, for defining global gridded distributions of cloud (by layered types) and cloudfree information from Global Area Coverage (GAC resolution) AVHRR data. Cloud analyses are based on pixel-scale classifications into four generic types, which include three thermally distinct opaque cloud types and semitransparent cirrus. The latter, when overlaying lower opaque clouds, is so identified. Classifications put each pixel in one of four classes: (1) a cloud-filled single type, (2) a cloud-filled mixture of cloud types, (3) partly cloudy, or (4) cloudfree. The basis for the development of CLAVR-2 was the initial CLAVR-1 algorithm, with its classifications for 2x2 pixel arrays, which successfully produced gridded global distributions of Total Cloud Amount and gridded CLEAR data sets. CLAVR-2 classifies data at the pixel scale, and generates summaries of cloud ensemble data by layered type. Sufficient detail on the MLCA is provided so that imagery users can apply or examine orbital products over regions of choice. Evaluation of selected orbital segments shows the method to produce pixel cloud classifications in qualitative agreement with satellite imagery. Quantitative evaluation of gridded global products will appear in a subsequent paper.

[1]Consultant to SMART Inc
[2]NOAA/NESDIS, Office of Research and Applications, 5200 Auth Road, Camp Springs, MD
[3]Scientific Management & Applied Research Technologies, Inc., Lanham, MD
[4]Private Consultant

AUTOMATED GENERATION OF GLOBAL CLOUD DATASETS FROM POLAR ORBITING SATELLITES PART I: CLAVR-2 PIXEL-SCALE MULTIPLE LAYER CLOUD ANALYSES (MLCA)

P.A.Davis, L.L.Stowe, Gang Luo, E.P.McClain , A. K. Heidinger

ABSTRACT

1.0 INTRODUCTION
1.1 Background
1.2 Remote Sensing Demands
1.3 Rationale
1.4 System Overview

2.0 PHYSICAL BASIS FOR CLOUD CLASSIFICATION THRESHOLDING
2.1 Cloud Type Classifiers
2.2 Basis for Nighttime Semitransparent Cirrus Classification
2.3 Basis for Daytime Semitransparent Cirrus Classification
2.4 Basis for D34 Thresholds for Opaque Low Stratiform Cloud
2.5 Basis for Cloudfree BTD DT3 (Ch.3 With/Without Solar Input)

3.0 SEQUENTIAL METHODOLOGY OF CLOUD CLASSIFICATION PROCEDURE
3.1 Initial Nighttime Generic Cloud Classification
3.2 Initial Daytime Generic Cloud Classification
3.3 Orbital Subswath Area Analysis
3.3.1 Definition of CLEAR T4
3.3.2 Semitransparent Cirrus (no underlying clouds)
3.3.3 Layering and Labeling (opaque clouds)
3.3.4 Cirrus with Underlying Opaque Cloud
3.3.5 Reclassification Restoral (PARTLY CLOUDY to CLEAR)

4.0 MLCA ORBITAL OUTPUT EVALUATION
4.1 Orbital Segments and Gross Generic Cloud Types
4.2 Evaluation of MLCA Orbital Image Samples

5.0 CONCLUSIONS AND PLANS
6.0 ACKNOWLEDGMENTS
7.0 APPENDIX
8.0 REFERENCES
TABLES
ILLUSTRATIONS

AUTOMATED GENERATION OF GLOBAL CLOUD DATASETS FROM POLAR ORBITING SATELLITES PART I: CLAVR-2 PIXEL-SCALE MULTIPLE LAYER CLOUD ANALYSES (MLCA)

1.O INTRODUCTION

1.1 Background

Satellite coverage has provided global imagery depicting the distribution of cloudiness and its large scale organization since 1960. Progress in automated real-time objective analyses of the satellite cloud information has been very slow, however, especially in terms of the operational global environment. Three major global nephanalysis programs from satellite data include the Nimbus-7 dataset (Stowe et al. 1986), the RTNEPH program (Hamill et al. 1992) and the ISCCP program (Rossow et al. 1993). The latter two continuing programs make use of AVHRR (Advanced Very High Resolution Radiometer) data from NOAA's polar orbiting operational satellites, but use other data as well. Only the RTNEPH analyses are performed in real time. There have been other earlier programs that used multichannel AVHRR measurements (e.g., Coakley and Bretherton 1982; Arking and Childs 1985; Chou et al. 1986; Saunders and Kriebel 1988), but these programs did not address real-time global coverage as was done in CLAVR-1 (Stowe et al. 1991 & 1998), the predecessor of CLAVR-2. Sixteen years of data based on the CLAVR-1 algorithm have been processed under Phase A of the Atmospheric Pathfinder program (PATMOS-A). The techniques developed for CLAVR have been applied to the afternoon NOAA polar-orbiting satellites, with all five channels of the AVHRR instrument (0.63, 0.83, 3.7, 10.8, 12.0 μm) used in the algorithms. AVHRR data resolution is either LAC (Local Area Coverage) at about 1 km near nadir, or GAC (Global Area Coverage), sampled at about 3x4 km resolution (the average of four of every five LAC pixels on every third scan line). Only GAC data are available for global operational coverage.

Products from CLAVR-1/PATMOS-A include $(110\ km)^2$ global gridded CLEAR and CLOUDY radiance datasets and Total Cloud Amount, but without specific distinction by type or layer. CLAVR-1 algorithms provide cloud classifications for each GAC 2x2 pixel array. That array decision is then applied to each of the four pixels in the array, resulting in an excessive number of "MIXED" pixels which may be clear, partly cloudy or cloudy and contributing to biases in the estimated cloud amount (Vemury et al, 1998) and (Stowe et al, 1998). To avoid these problems, CLAVR-2 algorithms address and classify individual GAC pixels.

1.2 Remote Sensing Demands

Information sought from satellite multispectral remote sensing includes not only cloud amounts and heights (tops and bases), but such cloud optical properties as optical thickness and particle size as well. Such information provides input and validation for numerical models dealing with the changing thermodynamic state of the atmosphere and the global hydrologic cycle. The associated radiative forcing on the atmospheric energetics cannot be assessed thoroughly without sufficent cloud distribution information to enable determination of instantaneous radiative flux distributions from the Earth's surface throughout the atmosphere.

Specific requirements for the overall CLAVR program were enumerated largely by NOAA's National Centers for Environmental Prediction, NCEP and called for a real-time operational estimates of the horizontal and vertical distribution of liquid water and ice in the atmosphere. This paper describes the techniques used for identifying layered amounts of cloud. Whereas the original requirement for real-time operational analysis is no longer imposed, the capability for meeting such a demand has been maintained in the software development. Consideration of all requirements for this remote sensing study led to the objectives adopted for the CLAVR-2 algorithms, which are summarized below. Meeting these objectives in global analysis while also meeting other user needs is very demanding on the processing system. Consequently, algorithm simplicity has been emphasized; and that simplicity has been maintained in procedures for radiometric determination of partly cloudy contributions to total cloud amount.

CLAVR-2 objectives for meeting requirements include:

- o Automated twice-daily pixel classifications by thermally layered opaque cloud types and semitransparent cirrus (with identified underlying backgrounds).

- o Multispectral radiances, brightness temperatures, and albedos defined for all labeled pixels, each identified by generic cloud type(s), by cloudfree surface type, or as partly cloudy.

- o Appropriate pixel classification groups and summarization of ensemble radiances by each type for gridcell definition of cloud properties (amount, height/pressure, semitransparent cirrus emissivity, temperature, effective particle size, and optical thickness).

- o Radiometric determination of partly-cloudy fractional contributions to total cloud amount of each layered opaque cloud or semitransparent cirrus type.

- o Assignment of pertinent temperature/moisture profiles to each grid cell for user assistance in deriving cloud properties and calculating radiative flux profiles.

The last three objectives are addressed during the mapping stage (Part II), whereas the first two objectives

are addressed in the the analyses of this paper (Part I).

The cloudfree grid data are needed both in cloud pixel classification and in pixel ensemble analyses, including determination of cloud amount. Classification at the pixel level preserves a satellite image representation of the cloudiness both for algorithm validation studies and for the preservation of organized cloud patterns that could be useful in deriving other products.

1.3 Rationale

To cope with the objectives laid out for CLAVR-2, certain processing philosophies have to be considered for the analysis of the AVHRR pixel data. These six philosophies deal with pixel radiance uniformity, field-of-view (FOV) cloud cover, cloud type, cloud test thresholding, and variabilities of optically thin cirrus, and analyses of pixel ensembles.

a) Estimating pixel radiance uniformity*:* As the sample variance within the GAC pixel is unmeasured, an estimate is made of its nonuniformity. The simplest option is to assume that the variability among adjacent pixels can be transferred downscale as representative of the GAC pixel itself. Thus the estimate of nonuniformity is based on the differences, in emittance or reflectance, between each GAC pixel and its three closest neighbors during the initial processing along a scanline pair. This estimate is subject to (1) an erroneous assessment of uniformity when the pixels have the same degree of nonuniformity and (2) an erroneous assessment of nonuniformity when pixel differences are large but individual pixels are uniform.

b) Characterization of Pixel Cloud Cover: The fractional cloud amount within the FOV is not strictly determinate quantity, at least not from any single spectral pixel measurement. Subresolution thermal ambiguity exists between cloud amount, cloud temperature, cloud height, and emissivity/optical thickness. Pixel FOV cloud cover has been defined initially in terms of four classes: CLEAR, PARTLY CLOUDY, CLOUD, or MIXED CLOUD. Both of the last two cloud classes in CLAVR-2 indicate complete pixel FOV cloud cover. The CLOUD class signifies that one generic type is viewed, whereas MIXED CLOUD implies a mixture of two or more generic cloud types. Fractional cloud amounts of each type are defined only after mapping in grid cells and must include contributions from pixels that were classified PARTLY CLOUDY, i.e., incomplete cloud cover.

c) Initial Cloud Typing: Although reflectance is a powerful tool for cloud detection, including those clouds beneath semitransparent cirrus, and plays a significant role in the derivation of cloud optical properties, the thermal emission channels must be emphasized for automated initial cloud typing. All cloud data are classified into one of four generic types: three thermally distinct opaque cloud types, each of which can be subdivided on the basis of cloud top temperature, and one semitransparent cirrus (ice cloud) type, with underlying surface type specified. The brightness temperature difference tests used in typing are analogous to the spectral signatures used in CLAVR-I (Stowe et. al. 1998).

d) Classifying with Thresholds: For cloud (or cloud amount) and cloud-free pixel classifications, decisions are based on background information derived from ensembles of like pixels. Brightness temperature difference thresholds applied to individual pixel cloud tests actually are designed to be appropriate for ensembles of pixels from a variety of typical atmospheric and surface conditions over the globe. They will not always hold true for specific individual pixel decisions for particular atmospheric/surface conditions. Some degree of statistical uncertainty is associated with any threshold. Allowance for part of the uncertainty is achieved by establishing double thresholds that encompass most of the single threshold uncertainty. A double threshold is not sufficient for semitransparent cirrus, mainly because of variable contributions from lower opaque boundaries. Each ensemble of semitransparent cirrus pixels must be associated with additional surrounding bounds (thresholds) that are linked to the temperature of the underlying surface (cloud or Earth).

e) Coping with Cirrus Variability: Optically thin cirrus represents the only semitransparent cloud type stipulated.. Initially, only a single semitransparent cirrus classification of CLOUD is made, regardless of lower boundary. However, even over a single uniform lower boundary, pixels classified as cirrus can have wide variations in cloud temperature and microphysical properties. Despite this variability, only a single average gridcell cirrus layer is considered when pixel ensembles are analyzed initially. Subsequently, separate semitransparent cirrus averages are obtained for each ensemble subset linked with radiances contributed from an identified lower boundary, either a lower opaque cloud top or the Earth's surface.

f) Pixel ensemble analyses:

While this paper deals with pixel-scale cloud classifications, the methods used here inherently rely on large ensembles of pixels to retrieve meaningful cloud characteristics. The initial cloud classifications made for each pixel are subject to a reclassification procedure based on the ensembles of pixels taken from a much larger region called the subswath area described in Section 3.3. This is especially true for the identification of the contributing cloud types to MIXED CLOUD pixels which is impossible to do from observations of individual pixels. This approach is needed to layer clouds or to cluster semitransparent cirrus pixels with the appropriate lower boundary (i.e. the Earth's surface or opaque cloud tops).

1.4 System Overview

This paper (Part I) covers the first of the two major CLAVR-2 algorithms: the pixel-scale Multiple Layer Cloud Analyses (MLCA). In switching from the CLAVR-1 2x2 array approach to the CLAVR-2 pixel approach, and in expanding from the former's Total Cloud Amount to the latter's multilayered cloud type approach, changes have arisen in cloud classifications, cloud tests, and cloud test sequences. The physical basis for the revised CLAVR-2 system is discussed in the next section; all procedures are consistent with the rationale set forth above. Inputs to the MLCA processor include processed satellite data outputs from CLAVR-1, equal-angle surface type databases (land/water at 1/16 deg, snow/ice at 1/3 deg, desert land at 1/6 deg), and half-monthly or monthly averaged gridded CLEAR data from the Clear Radiance Data Sets of CLAVR-1 (CRDS1) , clear polar data from previous CLAVR2 runs, or from monthly PATMOS-A clear radiance summaries. The clear radiance data are averaged into overlapping zonal data blocks extending up to 45^{o} in longitude. The SNOW/ICE and DESERT databases were added to CLAVR-2 to aid in cloud discrimination in the presence of such radiatively different background surfaces. SNOW/ICE was specified from SSM/I microwave data (Ferraro et al. 1996) from another satellite platform, and the DESERT database was derived primarily from several of the Olson World Ecosystem (1992) types. The gridded time-averaged CLEAR radiance data provide the information needed for analysis in the absence of real-time cloud-free observations with the orbit being processed.

Outputs from the MLCA include orbital subswath area $(330\ km)^2$ data statistics (stored digitally in Subswath Data Files) and the pixel image data, including all pixel classifications, calibrated pixel radiances, and location-illumination-viewing geometry. The outputs from the MLCA become inputs for the CLDS (Cloud Layered Data Sets) of Part II.

2.0 PHYSICAL BASIS FOR CLOUD CLASSIFICATION THRESHOLDING

2.1 Cloud Type Classifiers

There are two aspects to cloud classification thresholding: cloud detection and cloud typing. Both functions are combined into a single approach in the MLCA. In order to derive useful cloud optical properties, both cloud type and cover within a pixel are needed. The requirement for cloud typing, including semitransparent cirrus, has led to thresholding in terms of the brightness temperature difference as well as the Ch.4 brightness temperature and the Ch.1 or Ch.2 daytime reflectance. The detection aspect is handled by assigning each pixel's cloud cover to one of four classes:

- o CLEAR (CW=Clear Water; CL=Clear Land; CS=Clear Snow/Ice)
- o PARTLY CLOUDY (PC-x; x=generic cloud type, see Table 1)
- o CLOUD (single generic cloud type: G,H,M,or L of Table 1)
- o MIXED CLOUD (two or more generic cloud types, opaque dominant)

The latter two classes represent cloud-filled pixels. For each pixel's cloud class, cloud type thresholding is used to identify the generic cloud types from the AVHRR thermal channels. The four generic types are listed in Table 1. Three of the types: G, M, and L, are considered opaque (O). The type of opaque cloud in partly cloudy pixels cannot be determined. The fourth type, semitransparent cirrus (H),is further classified by the type of overlying lower opaque surface.

Table 1. Radiometric Generic Cloud Types

G: Glaciated Opaque, Cold Top
H: Semitransparent Cirrus; Highlevel
M: Mixed Phase; Midlevel
L: Liquid (Water); Lowlevel

[Types G,M,L treated as opaque]

Thresholding in the MLCA, as well as in other techniques to define cloud cover class and cloud type, is typically defined from a top-of-the-atmosphere two-channel Brightness Temperature Difference (BTD) as a function of the Ch.4 brightness temperature (T4). Thresholds established on a sound physical basis and backed by radiative calculations should yield classifications that can be subjected to meaningful cloud property analyses. Uncertainties in mean thresholds depend on variabilities in atmospheric profiles and in surface emissivities. The use of cirrus cluster zones thresholds described in the next section combine both the spectral signature tests with clear-sky contrast tests with the clear-sky information being derived from the subswath area analyses or other a priori data. Spatial tests, used primarily for detecting opaque cloud cover and its uniformity, are usually defined by T4 and its variability (DT4) relative to the

cloudfree T4 and DT4. DT4 is used also in the PARTLY CLOUDY and the cloud-filled MIXED type classifications. The three AVHRR thermal channels (3,4,5) define three BTDs: T3-T5=D35, T4-T5=D45, and T3-T4=D34. Neither Ch.4 nor Ch.5 is significantly affected by solar radiation, so that only D45 (responsive to all cloud types) could be applied unchanged in Night and Day algorithms. D35 (for type H) and D34 (for type L) have been restricted to the nighttime. Another type of daytime brightness temperature difference, DT3, expresses the difference between the apparent (observed) daytime Ch.3 brightness temperature and the daytime Ch.3 brightness temperature estimated for emission only (no solar reflectance). As guidance on the distinction between semitransparent and opaque cirrus, a cloud-filled pixel is considered opaque if the mean cirrus physical temperature is 233 K or less at an optical thickness of 3.7 or more at 10.8 μm. An empirically defined upper limit on T4 (241 K) is used in conjunction with D45 as a first estimate to identify opaque ice clouds. Cloudy pixels with T4 > 241 K likely include contributions from tops of mixed phase or water clouds. However, colder clouds with sufficiently elevated BTDs may be semitransparent ice clouds. With semitransparent cirrus the underlying surface contributes to the measured signal. Therefore, complete cirrus classification must include identification of the underlying opaque surface. Due to the importance of this automated classification, the next two sections describe in some detail the physical basis for these semitransparent classifications using D35 and D45 as well as lateral cluster zone bounds that are linked to the underlying lower boundary. The object is to define the probable cluster area for semi-transparent cirrus within T4, D35 or D45 space.

As was described by Stowe et al (1998), a series of tests using the spectral, spatial and clear-sky contrast signatures in the measurements for all five channels in the AVHRR can reliably detect the presence of cloud. To extend this technique to cloud typing, these tests and their application were modified. The application of these tests is covered in Section 3 with supporting details provided in the appendix. A brief review of the main cloud classification tests is presented below. The thresholds used by these tests are based on extensive simulations of clear conditions and of cloud BTD's as a function of T4, optical thickness, and surface emissivity, or are derived from zonal block time-averaged observations. Final refinements or subclassifications are made during the subswath area analysis.

- The Glaciated Opaque Cloud Test (**GOCT**) uses D45 along with appropriate thresholds and cloudfree surface temperatures to distinguish optically thick glaciated clouds(G) from semitransparent cirrus (H).
- The Liquid Stratiform Test (**LST**) performs a similar function as ULST in CLAVR-1 but uses

D34 instead of D35 to detect opaque liquid clouds.

- The semitransparent cirrus tests **CIRT**(night) and **FMFTH**(day) look for semitransparent cirrus(H) alone or over other opaque cloud types through the use of multiple threshold analysis based on T4 and D35(night) and D45(day).
- The Four-Minus-Five Test (**FMFT**), as its name implies, compares D45 against known thresholds to determine if pixels not satisfying CIRT or FMFTH are filled by opaque cloud.
- Thermal (T4) and reflectance (A1) cloud uniformity tests in CLAVR-2 are **CTUT** and **CRUT.** If observed DT4's exceed these thresholds, the pixels may be classified MIXED CLOUD during ensemble analyses.
- The Ch. 1 Albedo Contrast Test (**A1CT**) is used in the same manner as the RGCT in CLAVR-1 to test for clouds on the magnitude of A1 over both land and water.
- The reflectance ratio cloud test (**A2/A1**) is the same as RRCT in CLAVR-1 and tests for clouds, clear water, and clear land based on the ratio of A2 to A1.
- Background (cloudfree) pixel uniformity threshold tests, performed last, are BTUT and BRUT (daytime only). Background thesholds are defined from bimonthly average zonal block data.

An application of these tests in complete day and night algorithms is described in Section 3.0. Since the use of multiple thresholds was not part of CLAVR-1 and are most critical to the semitransparent cirrus classification procedures in CLAVR-2, the majority of this section will describe their physical basis. The last two parts of this section deal with additional differences between CLAVR-1 and CLAVR-2}

2.2 Basis for Nighttime Semitransparent Cirrus Classification

Inoue (1985 and 1987) has discussed the theory of using BTDs for cloud classification, including semitransparent cirrus. Baum *et al.* 1994, have addressed the application of BTDs to cirrus pixels at a variety of optical depths within an ensemble. Baum's simulated cirrus pixel data (personal communication, 1994) were used in this study for the development of automated procedures for the cirrus classifications. D35 (or T3-T5) is well suited for nighttime cirrus identification because of its wide range and sensitivity. The main reason for an enhanced magnitude of D35 for cirrus detection is the greater transmissivity of the cirrus at 3.7 µm (Ch.3) than at 12 um (Ch 5) caused by the spectral variation in single scatter albedo of cirrus particles, absorption due to water vapor and Planck function's sensitivity to temperature. Thresholding for D35, as well as for D45 (daytime cirrus detection), makes use of the cirrus model

calculations of Baum for cirrus crystals with a 20/20 length/width ratio and cover a complete range of optical thicknesses (between 0 and 50) at different cloud temperatures and a variety of surface/atmospheric conditions.

Figure 1a gives pair of curves (shaded between) for T4, D35 points of simulated cirrus pixels at two cloud temperatures (220 K and 238 K), for a mid-latitude summer profile having a 300 K surface temperature (cloud-free T4 = 290 K). Phase functions of Takano and Liou 1989 and Minnis *et al.* 1993 were adopted for the cirrus particles. A typical distribution of cirrus pixels within a 2.5 degree grid, is likely to be within the shaded area in Figure 1a. The hatched area shown below the shaded area is qualitatively shows the effect of increasing the crystal size for the same cloud temperature (238K). As particle size increases, the spectral variation of the single scatter albedo decreases between Ch3 and Ch5 causing the decrease in D35. As seen, D35 also decreases, for a given particle size, as the cloud temperature increases. The simulated points in each curve represent increasing optical thickness with decreasing T4, starting with zero optical thickness at the highest T4, where the two curves converge. At the origin, the curves for different cloud temperatures show the same slope. Even at other surface temperatures the cirrus cloud curves will converge to zero optical thickness with that same slope. As the optical thickness points increase, a maximum in the D35 curve is reached near 2.0. The orthogonal spacing between the same optical thicknesses on the two temperature curves reaches a maximum just before the optical thickness of 4.0. Beyond this point the clouds may be considered opaque, as evidenced by the nearly constant spacing between curves thereafter. Also, once the opaque cloud point is reached the T4's show little further reduction with increasing optical thickness. At the same time the D35 drops rapidly toward zero as optical thickness increases further.

In Fig.1b two curves are again given for the same two cloud temperatures, but now for a mid-latitude winter profile and a lower surface temperature (275 K with a cloud-free T4=273.7). Each curve represents a single cloud temperature and particle size, and the curves converge at zero optical thickness with approximately the same slope as in Fig.1a. The shaded area between curves with T4 greater than 241 K, although shifted toward lower T4 & D35, again represents the grid cell domain of semitransparent cirrus pixels over a single lower boundary surface temperature. As in Fig.1a, at each optical thickness (point) other than the zero origin, the colder cloud shows a larger D35 and a lower T4 than the warmer cloud for the same surface temperature. As complete opacity is approached, the T4s take on the values of the corresponding cloud temperatures and D35 approaches zero.

In both Figs.1a and 1b there are a pair of background thresholds, labeled CIRT1 and CIRT2 (CIRrus Thresholds #1 and #2), for all T4 exceeding 240K. CIRT1 connects all simulated points of zero optical thickness, and represents a threshold separating CLEAR from CLOUD-CONTAMINATED, with cloudfree pixels having smaller D35 for all T4 on CIRT1. This curve also derived independently from CLEAR radiance calculations for many different atmospheric temperature-moisture profiles. The threshold CIRT2 was originally constructed by linking all points with optical thickness (OT) 0.2 for the cloud temperature 238 K. To ensure ice particles, CIRT2 is redefined for points with OT=0.2 at the cirrus cloud temperature 233 K. The uncertainty in cirrus classification for optical thicknesses less than about 0.2, due to variability in pixel optical thickness, temperature, particle size, and geometric height and thickness, makes it impossible to reliably distinguish any of these properties for pixels falling between CIRT2 and CIRT1. The OT of 0.2 at 11 microns is sufficiently large to account for aerosol emission in channels 3,4 and 5. CIRT2 separates CLOUD-FILLED pixels (with D35 exceeding the D35 of CIRT2 at each T4) from CLOUD-CONTAMINATED pixels (between CIRT2 and CIRT1). In the uncertain domain between CIRT1 and CIRT2 the pixels are classed PARTLY CLOUDY, or possibly mixed phase.

In accordance with departures of specific atmospheric profiles from the mean profiles in simulations, observed cloudfree points T4, D35 may fall below CIRT1. In such cases, the existing CIRT2 actually corresponds to optical thicknesses greater than 0.2. The upswing of the CIRT1 and CIRT2 thresholds with increasing T4 (see Fig.1) expresses the average increase in atmospheric water vapor with increasing temperature which results in an enhanced D35 as the Ch.5 transmittance decreases.

As stated earlier, semitransparent cirrus pixels within a grid cell (especially those with T4 greater than 241K) are likely to scatter over the shaded/hatched areas (see Figs.1a & 1b) for a single lower boundary brightness temperature (cloud top or Earth's surface). The actual distribution of semitransparent pixels is likely to be greater than the simulated for two reasons: (1) there is more than one lower boundary surface contributing to the signals; and (2) each boundary surface offers a temperature distribution, not just a single temperature. Both of these expansion effects are handled in the semitransparent cirrus classification, for all pixels whose T4, D35 falls above the gross base threshold CIRT2, by establishing two lateral bounds Right and Left, approximated as linear, to encompass the possible pixels in the cluster associated with each identifiable lower boundary surface. The variability in each surface temperature is thereby taken into account. The right bound is the theoretical limit for simulated pixels above a surface with a temperature corresponding to the bound. The left bound is the lower limit set to encompass all semitransparent cirrus pixels above that boundary surface.

For the Right-side (upper) Cluster Zone Bound, labeled RCZB, the slope S_R is taken as the mean slope (-0.91) for all surfaces as the cirrus curves converge to zero optical thickness. RCZB would normally originate on or near CIRT1 (zero optical thickness) at the boundary brightness temperature and extend toward lower T4 and higher D35 with the slope -0.91. To allow for positive variations in surface T4, an increment of standard deviation is added to shift the RCZB. Only that portion of RCZB above CIRT2 actually constitutes the cluster bound for the right side.

The Left-side (lower) Cluster Zone Bound, labeled LCZB, also defined as a sloping straight line, originates on CIRT2 at a T4 that is 5 K lower than the T4 of RCZB at CIRT2 to approximate the variability in surface temperature. For this anchor point in T4, D35 space, D35 is tabled for all T4 on CIRT2. The target along the LCZB slope is a cloud pixel at an optical thickness of 3.7 and a temperature of 233 K. As a good approximation, the slope of LCZB between these two points is reasonably constant (-0.30) regardless of boundary temperature. [In the daytime, LCZB is defined in T4, D45 space and uses a variable sloping line between the two points.]

Figure 2 illustrates an example of the semitransparent cirrus cluster zone thesholds defined by CIRT2, RCZB, and LCZB for the lower boundary surfaces (OT=0.0) in both Figs.1a and 1b. In the first part of MLCA when T4SFC is defined by climatology, only one zone anchored by T4SFC is used. In the subswath analysis, where the temperatures of the surface and opaque cloud layers are identified, the nighttime cirrus classification is redone with multiple cluster zones as shown in Fig 2. For example, the colder of the two surfaces in Fig. 2 (T4 = 273.5 K) could be interpreted as an opaque lower cloud under the cirrus (H/L), which would result in a colder cluster zone. For the region between the two cluster zones and for the region of overlap, classification decisions involves codes for both cluster zones. The T4 scale in Fig.2 has been expanded relative to Fig.1 and data have been restricted to T4 greater than 240 K. Comparison of Figs. 1a & 1b with Fig.2 reveal that the shaded areas above T4=240 K in Fig.1 are incorporated well within the cluster zones illustrated in Fig.2. Each defined cluster zone allows for a surface temperature range as well as for larger cirrus particles. A decision on semitransparent cirrus pixels with temperatures below 241 K has been reserved for D45 both night and day mainly because of uncertainties in the accuracy T3 at very low temperatures. As illustrated in Fig 2., pixels falling into overlapping cluster zones may be classified in either of the cluster zones. The final classification of these nighttime pixels involves proximity to cloudfree LCZB or low-cloud RCZB and is described later. This process of initial nighttime semitransparent cirrus classification refers to the CIRT test, which is finalized in the subswath “cirrus” routine.

The lower limit of T4=241 K for semitransparent cirrus in Fig.1a or 1b recognizes that observed T4s exceed physical cirrus cloud temperatures because of transmission of radiation through the cloud. Giraud et al. 1996 indicate it is possible to obtain ice-cloud points at temperatures above 241 K in the lower left region of Fig. 2 as a result of warmer cloud or broken cloud cover. However, in either case the resultant cloud opacity would not fit the semitransparent mode. It is possible to have G clouds (ice) at temperatures above 241K, possibly up to T4 = 249 K, occurring at D35's less than that of a cluster zone bound for semitransparent cirrus.

2.3 Basis for Daytime Semitransparent Cirrus Classification

Since the reflected sunlight in channel 3 increases the complexity of cloud classification using D35, the daytime cirrus classification was performed using D45. The physical mechanism for enhanced D45 in the presence of cirrus are the same as in D35 and include the spectral variation in both cloud optical properties and the absorption of water vapor. Since the spectral variation between channels 4 and 5 is much less than 3 and 4, the resulting magnitudes of D45 are much less than D35. Another difficulty in using D45 is that the signal from cirrus can be of the same order of magnitude as D45 caused solely by clear-sky water vapor absorption. The same cirrus pixel modeling that was performed for D35 (Baum, 1994) was calculated for D45 as well and served as the basis for the development for the daytime cirrus classification.

Figure 3 illustrates the daytime cirrus classification methodology and is analogous to Fig. 2 for the nighttime cirrus classification. Two threshold curves, FMFT1 and FMT2, are shown in Fig 3 and provide the same function as CIRT1 and CIRT2 in Fig 2. The increase in FMFT1(Four Minus Five Temperature threshold) with T4 is due to the increase in water vapor with increasing surface temperature. The threshold FMFT2 corresponds closely with CIRT2 for D35, where the thresholds passes through the points with OT=0.2 for an ice cloud at the temperature 233 K. However, the threshold FMFT1 does not pass through the cirrus points for zero optical thickness as did CIRT1. Rather, the FMFT1 curves are defined as the upper envelope of many cloudfree simulations for a variety of atmospheric profiles (Stowe et. al., 1998)and are tabulated rather than curve fitted so as to best represent the envelope of simulated points. The FMFT1 falls below the cirrus OT=0.0 points (unlike CIRT1). The reason for the displacement of FMFT1 is the response of T4-T5 to other clouds in addition to the cirrus. Most of the

opaque cloud responses occur at relatively small D45. The procedure described here for daytime semitransparent cirrus classification is called FMFTH.

Figure 3 illustrates the two D45 lateral bounds RCZB (fixed slope) and LCZB (variable slope) for the two surface temperatures used in Figs. 1a and 1b. The determination of the lateral cluster zone bounds RCZB and LCZB for D45 differs from that for the D35 cluster zone bounds. Here the observed mean surface T4 on the FMFT1 curve is used as the origin for both lateral bound thresholds. The RCZB is again given the limiting slope (-0.22 for the calculations used in Section 2.2) of D45 versus T4 for small optical thicknesses.

Unlike the RCZB, the LCZB has a variable slope and two anchor points are needed for its definition. As with the RCZB, the first anchor point is the observed mean surface T4, T4SFC on FMFT1. The second anchor point, at T4=241, is D45 = THH where THH is defined as the intersection on T4 = 241 K of the line formed by T4SFC and the point in T4, D45 space corresponding to cirrus cloud with a temperature 233 K and optical thickness 3.7. The point THH can be approximated as a function of T4SFC.

$$THH = 0.57(T4SFC - 241) + 0.2 \qquad (1)$$

Although T4=241K is the minimum allowable T4 for initial semitransparent cirrus classification, the LCZB extends to much lower values of T4 to minimize the misclassification of opaque ice clouds as semitransparent cirrus.

In addition to the RCZB and LCZB in Fig. 3, another threshold is defined to distinguish pixels that are snow/ice from opaque ice clouds. This threshold for snow/ice classification is defined for all T4 < 241 with D45 < THG where THG is given as

$$\text{THG} = 0.0337\text{SATZ} = 0.813 \qquad (2)$$

for satellite zenith angles (SATZ) greater than 30 degree otherwsie THG is 0.2. The above empirical expression was derived from the data of Dozier and Warren (1982) to account for the increase in Channel 5 emissivity with SATZ. Pixels falling into this zone are classified as snow/ice, otherwise they are classified as opaque ice cloud.

In the implementation of the daytime FMFTH semitransparent cirrus test, pixels falling into the shaded regions are classified as semitransparent cirrus (H) over a lower surface defined by the corresponding anchor point on FMFT1. For pixels falling within overlapping shaded regions, the determination of the lower boundary type is accomplished through use of an A2/A1 test. Pixels falling beneath the LCZB but above the FMFT2 are classified in the subswath area analysis (Section 3.4). For pixels falling between FMFT1 and FMFT2, a partly cloudy classification or a noncirrus classification is made.

2.4 Basis for D34 Thresholds for Opaque Low Stratiform Cloud

The D35 has been used as a test for uniform low stratus at night (Stowe *et al.* 1991 & 1998) because of the absence of solar reflectance data. Other users (e.g., d'Entrement 1986; Baum et al. 1994) have used the D34 for this analysis test as well as for modeling water clouds for comparison with measurements. Both D34 and D35 are limited to the nighttime because of the Ch.3 response to solar radiation as well as to thermal emission. D34 was adopted for low cloud thresholding in CLAVR-2, with D35 reserved for the semitransparent cirrus check. The D34 signal is depressed to an increasing extent from positive to negative as T4 decreases and optical thickness increases for water clouds, especially those with relatively small drop sizes. The reversal in D34 is associated with the larger single scattering albedo for Ch.3 than for Ch.4.

The cloud/no-cloud threshold was first defined over the ocean surface by simulation, using cloudfree radiative calculations for many observed atmospheric profiles. Curve fitting for the CLEAR data points, simulated for a variety of cloudfree T4s, successfully led to D35 and D34 thresholds over the sea surface (McClain et al. 1989). Data points (T4, D34) that fall below the threshold are classified as CLOUD L, but those above the threshold are considered cloudfree unless classified differently by other tests. The threshold for D35 used in CLAVR-1 over the ocean was labeled ULST. After subtracting a constant that was determined empirically to capture the impact of the lower emissivity of land, a reduced ULST is applied over land with the added provision that $271 < T4 < 289$ K. In this study with D34 we chose the labels LST/OCN, LST/LND, and LST/DES to represent the thresholds over OCEAN, LAND (nondesert), and DESERT. As in CLAVR-1, the critical threshold is LST/OCN, with the other thresholds modified with surface type.

Figure 4 illustrates the modeled T4, D34 thresholds for ocean, land, and desert surfaces. Also shown is the T4, D35 CLAVR-1 threshold ULST over the ocean. The more pronounced rise in ULST35

compared with LST at higher T4s results from greater attenuation by water vapor in Ch.5 than in Ch.4. The threshold LST for a given lower boundary surface is expressable as

$$D34_{sfc} = f(T4) - C_{sfc} \quad (3)$$

where f(T4) is some function of T4 with coefficients that depend on the atmospheric spectral transmissivities for Chs.3 and 4. With the exception of surface elevation impacts, f(T4) embodies the average effect of atmospheric transmittance on the cloudfree threshold regardless of the underlying surface type. C_{sfc} is a constant for any given surface emissivity (over the ocean C_{sfc}=1 but it increases with declining surface emissivity. The empirically-determined function f(T4), usually based on simulations, could be expressed analytically, but such formulations are restricted to particular ranges of T4. It is much more convenient to tabulate the relationship as has been done for the double thresholds CIRT1, CIRT2, FMFT1, and FMFT2 (see Table A-2). However, instead of listing double thresholds for this test, two different BTD thresholds, LST/OCN (CLAVR-2) and ULST35 (CLAVR-1) are tabulated for the ocean surface. The change in threshold LST with a change in the lower boundary surface is accounted for simply by subtracting the appropriate C_{sfc}. To establish magnitudes for C_{sfc}, Ch.3 and Ch.4 brightness temperatures were calculated in accordance with stipulated surface spectral emissivities. The brightness and emission temperatures were calculated for the specific AVHRR instruments (see Appendix). Measurement simulations with the pertinent spectral response functions and equivalent widths led to estimates of the increase in C_{sfc} with the decrease in Ch.3 emissivity associated with surface type. It was assumed that the average atmospheric spectral transmissivity remained as a fixed superposition over the changes at the surface. At an average maximum surface temperature, it was calculated that C_{sfc} increases by an increment of 2 for about every 0.08 drop in Ch.3 emissivity relative to Ch.4. Until such time as C_{sfc} is a specified function of surface emissivity, only two C_{sfc} land estimates are currently used: 3.0 for vegetated land and 5.0 for sandy desert. Thresholds with these adjustments are illustrated also in Fig. 4.

Applications over the ocean at night occasionally result in individual pixels classified as CLEAR because D34 exceeded LST at the observed T4, even though colder than other surrounding cloudfree T4s. A likely cause of this problem (Baum et al. 1994) is the Planck effect at 3.7 µm, which exaggerates the increase in Ch.3 temperature and D34 when there are subresolution holes/breaks in an otherwise uniform opaque cloud cover. The D34 is elevated above the LST threshold, perhaps even shifting from negative to positive. To avoid this difficulty, a secondary threshold is applied at night, but only to the ocean with T4 above 271K. If the pixel D34 falls below this secondary threshold but above LST/OCN, it is classed as PARTLY CLOUDY instead of CLEAR. This secondary threshold, LSTH2, is included in Table A2 in the

Appendix.

2.5 Basis for Cloudfree DT3 (Ch.3 w/wo Solar Input)

The estimated Channel 3 daytime brightness temperature difference DT3 represents the excess of the observed 3.7 um brightness temperature (T3) relative to the brightness temperature arising solely from thermal emission (T3e), or DT3 = T3 - T3e. If the observed daytime D35 exceeds that of the corresponding point on CIRT2 by DT3 or more, then the daytime application of the D45 semitransparent cirrus thresholds is corroborated.

The observed spectral radiance corresponding to the reflected solar irradiance can be expressed in Planckian form as

$$R_3 = B_3(T3) - B_3(T3e) \qquad (4).$$

The term T3e is estimated for an opaque uniform lower boundary by regressing nighttime observations of T3 on T4 and T5 as the latter are unaffected by solar reflectance in the daytime. Regressions should be applied separately for each cloudfree surface type. The R_3 so obtained may then be applied to the estimation of the top-of-the-atmosphere bidirectional equivalent-isotropic albedo for Channel 3

$$A_3 = \pi R_3 / (\mu_o d^2 S_3) \qquad (5)$$

where μ_o is the cosine of the solar zenith angle, d is the ratio of the mean to the actual earth-Sun distance, and S_3 is the filtered solar spectral irradiance at normal incidence and mean distance. Inasmuch as CLAVR-1 has only used a regression over the ocean and regressions for each type of land surface have not yet been implemented, it was necessary to estimate DT3 by working in reverse. In other words, nominal estimates of A_3 were used from key surface types to define R_3 in (5). Given a typical emission temperature (T3e), R_3 can then be converted through (4) to DT3, the brightness temperature increase due to solar reflectance.

3.0 SEQUENTIAL METHODOLOGY OF CLOUD CLASSIFICATION PROCEDURE

3.1 Introduction

After ingestion of 96 GAC scanlines, covering about 300 km along the orbit track., pixel processing is done along each pair of consecutive scanlines. As each pixel is examined, uniformity measures and BTDs are formed. Table 2 summarizes the three major stages of pixel classification in the MLCA imager algorithm. Tests listed within each stage also are arranged sequentially.

Table 2. Sequential Procedures in MLCA Pixel Processor

Initial Nighttime Generic Cloud Classifications
TESTS: GOCT, LST, CIRT, FMFT, CTUT, BTUT

Initial Daytime Generic Cloud Classifications
TESTS: GOCT, FMFTH, A1CT, A2/A1, BTUT&BRUT

Final Orbital Subswath Area Classifications
- o Definition of CLEAR T4 Thresholds for cirrus.
- o Layering and labeling (opaque clouds)
- o Definition of cloud-top temperatures below cirrus and semitransparent subclassifications.
- o PARTLY CLOUDY to CLEAR reclassification (restoral) and final data statistics.

The first two stages of the algorithm are the nighttime and daytime initial classifiers. Brightness temperature differences involving Ch.3 are not used in the daytime except to corroborate thin cirrus identifications. They are replaced with reflectance threshold tests. Thermal nonuniformity tests are supplemented with reflectance nonuniformity tests. The few pixels that are impossible to classify unambiguously,(ie specular reflectance regions at low sun), are discarded as in CLAVR-1 so as to avoid an "undecided" category after analysis. Classification codes assigned during these initial stages are not finalized until the subswath area analysis. Figures A1 and A2 in the Appendix show the details of the initial decision (classification) tree, and indicate each output code and the related cloud type(s).

Closure on the initial classifications is accomplished in the final stage of subswath area analysis. For that analysis, six subswath areas are defined cross-track for each swath of 96 scanlines; these have cross-track scanspot widths of 60, 72, 72, 72, 72, and 61 pixels. Each area is large enough for good probability of containing some CLEAR pixels and sufficient cloud pixels for meaningful layering and labeling. All pixels within each subswath area are tagged with the ID for that subswath area for post-MLCA analyses.

Upon completion of analyses over the six subswath areas and their data storage, all analysis procedures are repeated sequentially for the next swath of 96 scanlines along the orbital track.

3.2 Initial Nighttime Generic Cloud Classification

Nighttime cloud tests employ data from all three AVHRR thermal channels, but there is a potential problem in the definition of "nighttime" because Ch.3 responds both to emission and reflected sunlight. Nighttime here includes all solar zenith angles exceeding 84.3 degrees, with the assumption that beyond 84.3 deg there is insufficient sunlight to disturb the nighttime testing. Empirical checks suggest, however, that on occasion there is sufficient solar energy out to solar zenith angle 86.0 to adversely affect nighttime thermal tests involving Ch.3. Also, at night it is necessary to check the Ch.1 (0.63μm) radiance for the possibility of light leaks entering the AVHRR system when the satellite is in sunlight, Stowe et al (1998).

The flow chart (decision tree) for the nighttime in Fig.A1 shows all of the key tests in rectangles on the left side of the decision tree with the exception of CTUT, a thermal nonuniformity cloud test that is applied only after a cloudy decision has been made. Classifications (Cloud Codes) appear in double framed rectangles with labels attached.

Table 3 lists all key nighttime tests in the order of their application. Listed BTD parameters and thresholds were discussed in Section 2. The application of the GOCT (T4,D45) is the same for land or water, day or night. At night this test is followed by the two tests involving Ch.3; the FMFT test and the nonuniformity tests complete the sequence.

Table 3. Nighttime Cloud Test Sequence

TEST	NAME	MAIN PARAMETERS	THRESHOLDS
GOCT	GLACIATED OPAQUE CLOUD	D45, T4, T4CLR	241 K, THG, THH
LST WARM RANGE COLD RANGE	LIQUID STRATIFORM CLOUD	D34, T4, SFC TYPE	LST/OCN, Csfc LST H2
CIRT	CIRRUS (OPTICALLY THIN)	D35, T4, T4SFC	CIRT1, CIRT2, RCZB, LCZB
FMFT	FOUR MINUS FIVE	D45, T4	FMFT1, FMFT2
CTUT	T4 NONUNIFORMITY (CLD BKGRD)	DT4	3 K

BTUT	T4 NONUNIFORMITY (CLR BKGRD)	DT4, SFC TYPE	MONTHLY MEAN ZONAL DATA

The CLAVR-2 LSCT34 test is actually applied at three points in the algorithm. The first application, after GOCT, is for all T4 greater than 261 K. Secondly, after FMFT a cold cloud check is applied for the T4 range 241 to 261 K. Finally, over the ocean and after BTUT, a secondary threshold is applied for T4 greater than 271 K to check for a possible misclassified CLEAR.

3.3 Initial Daytime Generic Cloud Classification

The daytime algorithm incorporates data from all five AVHRR channels, including the short wavelength Ch.1 (.63μm) and Ch.2 (.86μm) bidirectional equivalent-isotropic albedos (see Eq.5 for A3). Both A3 and the Ch.3 brightness temperature difference DT3 are included in the testing. As the reflectance tests are not immediately definitive in terms of cloud type or layering, the two IR daytime tests are performed first so as to identify the opaque and semitransparent cirrus as early in the sequence as possible.

The flow chart in Fig.A2 in the Appendix gives the details of the daytime cloud classification test sequence, prior to subswath data analyses. Fig. A2 uses the same conventions as in Fig.A1. Table 4 lists sequentially the daytime pixel tests and thresholds.

Table 4. Daytime Cloud Test Sequence

TEST	NAME	PARAMETERS	THRESHOLDS (W/L)
GOCT	**GLACIATED OPAQUE, COLD-TOP**	**D45, T4, T4CLR**	**241 K, THG, THH**
FMFTH	**FOUR-MINUS-FIVE THIN CIRRUS**	**D45, T4, D35, DT3, T4SFC**	**FMFT1, FMFT2, RCZB, LCZB**
A1CT*	**REFLECTANCE A1 CLOUD TEST**	**A1, A3, A2/A1**	**A1:(30%/40%)**
A2/A1*	**REFLECTANCE RATIO CLOUD TEST**	**A2/A1, A3**	**A2/A1:(0.9/1.05)**
BTUT **BRUT**	**T4 BKGRD NONUNIFORMITY** **A1 BKGRD NONUNIFORMITY**	**DT4** **DA1**	**MONTHLY MEAN ZONAL DATA**

* A1CT & A2/A1 INVOLVE NONUNIFORMITY CLOUD TESTS CTUT & CRUT

The FMFTH test will use thresholds FMFT1, FMFT2, RCZB, and LCZB pertinent to each background surface temperature to classify semitransparent cirrus as long as D35, using the observed daytime Ch.3 temperature, exceeds CIRT1 by an amount greater than DT3, a table lookup value that depends on surface type (see Table 5). Actual DT3 values for any given reflectance depend strongly on background scene temperature. Therefore, by introducing minimal values of DT3 in Table 5, the warmer backgrounds for each type are stressed. Because of its low temperature, the largest value of DT3 is for sea ice, where a Ch.3 surface reflectance of 5% was assumed in accordance with Salisbury and D'Aria (1994). The calculations of DT3 for assumed reflectances were performed with Eqs.(4) and (5), as well as by appropriate conversion expressions for defining the brightness temperature changes for the stipulated Ch.3 spectral radiances (see Appendix).

As snow covered land is not explicitly included in Table 5, it could take on the DT3 either for land or desert (8-10 K), which is an appropriate value for Ch.3 reflectances of less than 2.5 percent at a background temperature of about 263 K.

Table 5. Ch.3 Temperature Adjustment (DT3) for Surface Reflectance

SFC TYPE	REFLECTANCE(%)	DT3(K)
OCEAN	2.5	3
SEA ICE	5.0	17
LAND	10.0	8
DESERT	17.5	10

3.4 Orbital Subswath Area Analysis

To this point, the processing described above have been performed at the individual pixel level, within a set of 96 scanlines. This initial phase served not only to detect the clouds but also to provide a phase-related classification by generic type. However the final decision on any cloud properties at the pixel level require information from the surrounding area. To meet the requirements for the CLAVR-2 analysis, we chose to examine subswath areas that were on the order of a magnitude larger then the final global grid size $(110\ km)^2$. In general, the subswath area must of sufficient size to

1) enable layering of the pixels of each opaque cloud type

2) include clear pixels and unobscured L and M type pixels to allow for subsequent fractional cloud analysis and definition of cirrus cluster zones.

In accordance with Table 2, pixels within a subswath area are subject to the following steps in analysis: (1) definition of a CLEAR T4, (2) identification of semitransparent cirrus occurring alone, (3) layering and labeling of opaque clouds, (4) identificaion of cirrus with underlying clouds, and (5) selective PARTLY CLOUDY to CLEAR reclassification.

3.4.1 Definition of CLEAR T4

Before semitransparent cirrus pixel ensembles can be defined, it is essential to define the cloudfree T4, i.e., T4CLR. Semitransparent cirrus signals cannot be interpreted without knowledge of the opaque lower boundary radiometric properties. If there are no CLEAR observations in the subswath area, and if no predictions of the cloudfree T4 are available, CLAVR-2 must use average gridded cloudfree T4 summaries. These may be obtained from the pertinent radiance summaries in the 16-year dataset of PATMOS (Pathfinder-Atmospheres program, Stowe et al. 1997). Means of the clear T4 so derived are referred to as T4CLR. The approach adopted is to store the gridded data within global zonal-blocks, arranged by surface type and zenith angle bin. Overlapping (in latitude) block sizes are typically 9 degrees of latitude by 45 degrees of longitude. Time averages are designed to give means every 15 days (half-month).

When there are observed CLEAR pixels, the average CLEAR T4 for each surface type in the subswath area is labeled T4BAR. T4BAR is the preferred temperature for subswath area analyses. Maxima and minima of PARTLY CLOUDY observations in the subswath area also are retained. If there are no CLEAR observations in the area, then T4BAR is set equal to the PARTLY CLOUDY maximum T4, plus 2 K. Otherwise, T4BAR is set equal to the appropriate T4CLR from the zonal block containing the subswath area.

3.4.2 Semitransparent Cirrus (without other cloud)

At night, all pixels falling above CIRT2 in Fig.2 are taken as representative of semitransparent cirrus, occurring either alone or above some lower opaque cloud. Given the cloudfree T4BAR (289.6 K in Fig.2) to define the cloudfree lower boundary, the cluster zone (between RCZB and LZCB above CIRT2) for cirrus without lower cloud is defined. Pixels below the zone between CIRT2 and CIRT1 are considered PARTLY CLOUDY cirrus. Establishment of this cluster zone is necessary for further subdivision of semitransparent cirrus over the areas not free of cloud.

During the day, the FMFTH test is applied for semitransparent cirrus. Fig.4 illustrates the cirrus alone

cluster zone above FMFT2 (for T4BAR again equal to 289.6 K). Once this critical cluster zone is defined in T4, D45 space, the more complex daytime analyses for cirrus over other cloud and for the other cloud without cirrus can proceed. With the substantial overlap of this cluster zone with other cluster zones from lower cloud, many of the pixels in the "cirrus alone" cluster may subsequently be reclassified as cirrus over lower cloud on the basis of reflectance data.

3.4.3 Layering and Labeling (opaque clouds)

All available opaque cloud decisions (G,M,L) are subjected to thermal layering. However, when D45 is used for semitransparent cirrus analysis there may be some pixels exceeding the FMFT2 threshold that will be assigned to opaque cloud codes (without any cirrus) after the final cirrus analysis. These pixels are not included in the layering process, but will be finally labeled with the appropriate layered code. The thermal layering, or subdivsion of a gross generic cloud type, is not essential prior to mapping, but has been performed in the MLCA for each subswath area. The layered results are applicable only to the given subswath area. In fact, the gross generic subswath statistics (without subdivision) for the M and L cloud types are sufficient for completion of the analysis of cirrus overlying lower cloud. In the absence of overlying cirrus, the subdivision of opaque types into distinct layers is required before the optimum derivation of cloud optical properties. Therefore, if one sought to derive optical properties (perhaps as a check) from data within the subswath area, the layering will be helpful.

Rules and methods for layering are somewhat arbitrary. An initial decision was to limit to three the number of independent layers of any one given cloud type within the subswath area (fewer for smaller grid cells). Layering was based on maxima in the frequency histogram (one-degree Ch.4 temperature bins) for all pixels with the same generic cloud type in the subswath area. Local maxima in frequency counts are identified, then checked statistically (in a manner very similar to that of Luo et al. 1995) to screen for significance. If significant layers overlap at the two-sigma level, they are combined. If further reduction in the number of layers is required, the closest layers are combined and the statistics are recalculated.

Total subswath statistics are accumulated as well for each generic opaque type. These statistics resemble those for a single layer but with typically larger variance. Unlayered residual M and L pixels with T4 more than two sigma greater than the warmest cloud layer mean are reassigned to PARTLY CLOUDY.

During the labeling process, all of the categories with an uncertainty in layer or type are reanalyzed after the layering. Each pixel must be (1) associated with a CLOUD layer of a particular type, (2) a MIXED CLOUD of two types, with one opaque type dominant, or (3) PARTLY CLOUDY. Labeling is the

assignment of the proper numeric code to each pixel. Labeling for the difficult MIXED class (Option 2) assigns one of six codes to the three dominant opaque cloud types (G, M, L). Each dominant type takes on only two of the six codes defined in Table 6. Note that G dominates Codes 51 and 53, M dominates Codes 52 and 55, and L dominates Codes 54 and 56. When gross generic statistics are formed for each type, the two mixed types for which the type is dominant are included. For example, with up to three layers allowed for type G (say, Codes 11, 12, 13), the gross generic class G would include Codes 51 and 53 as well, for a possible total of 5 codes. However, the MIXED types (e.g., 51 and 53) are not well suited for the direct derivation of optical properties.

Table 6. Opaque Cloud Codes for MIXED CLOUD Types

51: G (dominant) + cirrus(H)
52: M (dominant) + G and/or cirrus(H)
53: G (dominant) + lower opaque(L,M)
54: L (dominant) + higher opaque(G,M)
55: M (dominant) + L and/or cirrus(H)
56: L (dominant) + cirrus(H)

3.4.4 Cirrus over Underlying Opaque Cloud

In order to complete the clustering (subdivision within each RCZB-LCZB pair) and labeling of semitransparent cirrus, and eventually to define fractional cloud amounts from observed partial cover, the mean cloud top temperatures, T4L and T4M, of L and M cloud ensembles are needed. If T4L and T4M are not available after subswath layering and labeling, but there are PARTLY CLOUDY pixels, then the minimum T4 could be used to estimate the cloud top T4 (provided that the clouds are colder than the surface). Current software invokes simple defaults by setting T4L halfway between T4BAR and 263K (for T4BAR > 263K + σ). Similarly, T4M is set halfway between T4L and 243K. Otherwise, in the absence of L or M cloud without overlying cirrus, cloud-top T4s can only be defined wherever the data (from greater BTDs) tend to cluster on CIRT1 or FMFT1.

Having defined T4L and T4M for existing L and M cloud tops in the subswath area, it is possible to complete the subclassification of semitransparent cirrus by defining appropriate cluster zone boundaries in the same manner as was done for T4BAR of the cloudfree surface. Table 7 displays, after cluster subdivision and labeling, the cloud codes from the semitransparent cirrus analysis. In each group, the lowest cloud code is the coldest and the highest is warmest. As will be seen in the imaging, only the combined gross generic cirrus class has been plotted (i.e., codes 21, 22, 23, 61, and 62). However,

distinctions will be maintained when mapping or inferring optical properties.

Table 7. MLCA Semitransparent Cirrus Cloud Codes

CLOUD-FILLED CIRRUS OVER OPAQUE LOWER BOUNDARY

21: H/M Cirrus over M cloud
22: H/L Cirrus over L cloud
23: H Cirrus over Earth's surface

MIXED CLOUD TYPES WITH CIRRUS

61: 21 + 22
62: 21 or 22 + 23

PARTLY CLOUDY CIRRUS

82: 21 or 22 + CLEAR
83: 23 + CLEAR

3.4.5 Reclassification Restoral (PARTLY CLOUDY to CLEAR)

In the final step of subswath analysis statistics are generated for all observed cloud and clear classes. In addition, the PARTLY CLOUDY statistics, for the two cirrus and two opaque (L and UNKNOWN) PARTLY CLOUDY types, are reviewed for the primary purpose of performing a "thermal chopping" of those PARTLY CLOUDY pixels that are warmer than the surface, provided that the clouds are colder than the surface. There are two major reasons for performing the thermal chopping restoral (reclassification) of partly cloudy pixels to clear, prior to ensemble analysis. First, uniformity checks could be in error, because the desired uniformity within the GAC pixel is only estimated. Secondly, there may be an excessive number of partly cloudy pixels with brightness temperatures significantly higher than the clear pixels, due in part to faulty uniformity measures, so that the ensemble average, which is used in the radiometric balance approach to define cloud amounts (Part II), is shifted too high by the warmest pixels. The result is that no partial cloud contribution is made to the total cloudiness by the entire partly cloudy ensemble. If individual pixels were subjected to the radiometric balance approach, each pixel T4 above the mean clear T4 would lead to a CLEAR decision, just as in thermal chopping. Thermal chopping restoral is not performed if any **cloud** mean T4 exceeds the clear mean T4. Pixels exceeding the thermal limit for restoral, T4CHOP, taken here as the highest observed or estimated mean clear T4, must also be subjected to reflectance checks for daytime restorals over the ocean. No thermal chopping is done within the polar caps.

Once thermal chopping is completed and final labels and statistic revisions are completed for each subswath area, a variety of flags are added to the subswath data files, along with location information,

subswath ID, and beginning and ending scanlines.

4.0 RESULTANT ORBITAL OUTPUTS AND EVALUATION

The digital MLCA output is the data source for generating pixel-scale imagery and for mapping routines to produce datasets that include gridded global cloud amounts by layered types (Part II of this paper). Orbital digital segments, imaged from a 1C tape, encompass specific subswath areas, each with digital data summaries stored in Subswath Data Records. Locations of the subswath areas within the imaged orbital segment are known. Subswath digital records can be interrogated for digital image and algorithm evaluation, or used for special analyses by the user.

4.1 Orbital Segments and Gross Generic Cloud Types

For image analysis and evaluation, pixels in each of the four generic CLOUD classifications (G,M,L,H) and in the PARTLY CLOUDY (PC) class (PC-L,PC-O,PC-H) are grouped together into gross generic types. PARTLY CLOUDY labels refer to partly cloudy with L clouds (Code 71), partly cloudy with unknown opaque clouds (Code 72), and partly cloudy with cirrus (Codes 82,83). The latter category (see Table 7) actually may contain three partial covers of all three types: H/M, H/L, or H. Thus, the gross generic PARTLY CLOUDY group contains four possible cloud codes two of which contain cirrus. Each of the three opaque gross generic CLOUD types possibly contains five cloud codes: up to three possible layers of the single generic type and two possible MIXED CLOUD types that are dominated by the generic type (see Table 6). The gross generic cirrus cloud type also contains five codes (see Table 7): H/M, H/L, H, and two MIXED CLOUD combinations involving these types. Each of the five generic types (G,M,L,H,PC) become five single class gross generic types (GG,GM,GL,GH,GPC). Two additional classes are added: CLEAR WATER (CW), and CLEAR LAND or CLEAR SNOW/ICE (CL-CS). With the combination of land or snow/ice as a solid lower boundary, there are a total of seven classes for convenient correspondence with the rainbow color display. Details of the specific color bar chart adopted here for the MLCA color images of cloud classifications are summarized in Table 8. Each color (gross type) makes no distinction with respects to height, temperature, or reflectance variations within the class.

Table 8. Color Image Plan: MLCA Gross Generic Cloud Classification (COLOR-BAR SCALE: 0 - 850)

RAINBOW COLOR	COLOR-BAR NUMBER	GROSS GENERIC CLASSIFICATION	CLOUD CODES	DESCRIPTION
VIOLET	0	(CL-CS)	8,9	CLEAR LAND-SNOW/ICE
INDIGO	80	(CW	7	CLEAR WATER
BLUE	280	(GPC)	82,83,71,72	PARTLY CLOUDY
GREEN	480	(GH)	21,22,23,61,62	CIRRUS (± LOWER)
YELLOW	660	(GM)	31,32,33,52,55	MIDLEVEL;MIXED PHASE
ORANGE	750	(GL)	41,42,43,54,56	LIQUID, LOWLEVEL
RED	850	(GG)	11,12,13,51,53	GLACIATED OPAQUE

Figure 5 is a daytime color image of the gross generic cloud types with the color bar scheme of Table 8. The typical satellite images for Ch.4 (emission) and Ch.2 (reflectance) are illustrated for comparison. The gross generic type GG (red) coincides with the coldest and brightest elements in Chs.4 and 2, respectively. The gross cirrus type GH (green) appears quite cold (bright) in the Ch.4 temperature gray scale, but dull in Ch.2 reflectance, with variations according to the underlying background. Midlevel clouds GM may appear slightly warmer than GH clouds in Ch.4, but are brighter in Ch.2, unless M clouds are overridden by H clouds. Finally, the low clouds, GL, typically are dull (warm) in Ch.4 and bright (reflective) in Ch.2. PARTLY CLOUDY pixels are difficult to represent in a color image, as all types are given one color, giving partly cloudy pixels the false appearance of being cloud-filled. Thus, the light blue color for PARTLY CLOUDY gives the appearance of much more extensive cover than actually existed.

The next three-part figure (Fig.6) illustrates the potential usefulness of two reflectance measures, A1 and A2/A1, in the interpretation of widely-scattered daytime gross generic cirrus pixels. Figure 6a presents an observed scattergram of BTD T4-T5 against the Ch.4 brightness temperature for GH pixels observed in one subswath area of the image in Fig. 5 over the south-central USA (Orbit 489899, NOAA-11, 9-6-89). The subswath area had a southern border on the Gulf of Mexico. In this case L clouds were observed, as also were M clouds MIXED with G or H. The different cloud codes are represented by different point symbols. Points with the dotted circles are not actually GH pixels, but are partly cloudy cirrus only pixels. Cloud

codes result from the daytime semitransparent cirrus analysis described in Sections 2.3 (see also Fig.3) and 3.3, but for three different opaque lower boundaries (T4BAR,T4L,T4M). Note that the black diamond clusters separate around the cluster for H/L (Code 22). The warmer cluster (Code 62) is between H and H/L clusters, while the colder mixed cluster (Code 61) is between H/L and H/M. There is a very sizable overlap between the types H and H/L, especially where lower T4s are observed. Many of the pixels with T4 below 241 K were classed as semitransparent. Decisions on the presence of L below H clouds in the overlap region were based on reflectance data A1 and, especially, the ratio A2/A1.

Fig.6b illustrates A1 against T4 for all of the cirrus pixels. Although the partly cloudy pixels cluster on the warm end, as they should, it is noted that at the bottom of the distribution (pixels with albedos ranging between about 9 to 34 percent) are the thin cirrus occurring without lower cloud. The albedos increase with decreasing temperature, which corresponds with increasing optical thickness. The warmest code 23 pixels with albedos between 30 and 40 percent possibly should have been classified as H/L (code 22). The two A1 peaks near T4=246 and T4=270 for Codes 21 and 22 are typical of what might be observed over M or L clouds in the absence of cirrus. However, they occur about 10 K or more below the T4 observed for these cloud tops, which is consistent with the presence of cirrus.

Fig.6c illustrates the ratio A2/A1 against T4 for the same data points as 6a and 6b. Ratios between 0.9 and 1.1 are considered indicative of opaque cloudy (cloud-filled) pixels, so that here they are most representative of Codes 21 and 22. The nonlinear increase in the ratio above 1.1 pixels with increasing T4 for mostly Code 23 indicates decreasing optical thickness and possibly also decreasing cloud cover, which is characteristic of increasing contribution from underlying land. Ou et al., 1996, have recently discussed the use of A2/A1 in cloud analysis.

In cloudfree coastal regions a pixel could pick up radiances from both water and land (respective A2/A1 ratios less than 0.9 and greater than 1.1), leading to an ambiguous ratio near 1.0, which is typical of cloud. [A2/A1 also is useful in the distinction of sea ice, as well as dust plumes over cloudfree oceans.

Evaluation of the gross generic color imagery in complex situations can be hindered by the subswath area analyses performed prior to recombination into the larger image of the entire orbital segment. For example, when neighboring subswath areas consist of ensemble data just on opposite sides of a threshold, the resultant combined image may show a blocky pattern (i.e., sharp color differences across subswath boundaries). Such blockiness, or boundary artifact, is quite common when larger images are formed from a combination of adjacent independent local or regional analyses. Minor blockiness will not reappear when

data are mapped and gridded on a scale significantly smaller than a subswath area. If image distortion is pronounced, the analyses must be examined for problems.

One of the most important overall evaluation-validation tools are the global gridded monthly (or shorter period) mean maps of "pure CLEAR" parameters from CLAVR-1 or PATMOS climatological datasets (both ascending and descending modes). The CLEAR data for September 1989 were a key information source for testing CLEAR data from the CLAVR-2 algorithm and for spotting specific errors or anomalies in the analyzed CLAVR-2 cloudfree fields.

4.2 Evaluation of MLCA Orbital Image Samples

The quality of the CLAVR-2 cloud products ultimately depends upon the pixel classifications made in the MLCA algorithm. Several representative images are examined to assess features of the orbital classifications.

Figure 7 is a typical nighttime desert view over the region across Egypt and Saudi Arabia (Orbit 490102, descending, 9-6-89). This orbital GAC segment image shows the gross generic cloud classifications (8a), and the Ch.4 brightness temperature (8b). The cloud classification image looks fine except for one feature: low clouds (gold color) appear in the analysis along the Nile valley and near the eastern shore of the Mediterranean but not in the satellite T4 image.

Portions of this scene that appear to be CLEAR in the T4 image were plotted in Figure 8 in terms of the background sensitive LST test (for liquid (low) stratiform clouds) using D34 versus T4. In Fig. 8a all CLEAR DESERT pixels in the subswath area are plotted on the T4, D34 graph along with the OCEAN, LAND, and DESERT thresholds. Note that the distribution of CLEAR pixels above the DESERT threshold ends abruptly at this threshold, as it must. The comparison with the "cloud" points in Fig.8c suggests that all of the points with T4 above 290 K are part of the same distribution, including the tip consisting of a few points that exceeded the DESERT threshold near T4=293. Obviously, if the thresholds were lowered by an amount of the order of 0.5, there would be no cloud points over the desert. All of the points called cloudy that fell between T4s of 290 and 295 do not appear to be cloudy but are so labeled because they exceed the CLEAR LAND threshold. Similarly, the points in Fig.8b are called CLEAR LAND but certainly appear to be in the CLEAR DESERT pixel cluster. The logical explanation seems to be that the relatively few "LAND" pixels were erroneously classified. On the basis of their Ch. 3/4 emissivity differences, they should have been included with the DESERT pixels. [All of the CLOUD pixels with T4 less than about 290K and D34 above -1.0 must have been so classified by a test other than LST (probably from the logic

following the FMFT test).]

Several important conclusions are based on the LST results. First, as the original threshold fitting against simulated CLEAR pixels did not consist of the lower envelope of simulated points and included very moist atmospheres at the warmest end, it is likely that the threshold curves shown in Fig.3 were curved excessively toward higher D34 at higher T4. If the curves were more linear and lowered a bit, especially beyond about 290K, the warm "CLOUD" pixels over LAND and all "CLOUD" pixels beyond the DESERT threshold would have been classified as CLEAR. This would have been consistent with the image and clear nighttime T4s (all greater than 290K) for these pixels. Finally, the other "CLOUD" pixels over LAND would also have been classified as CLEAR if the surface type had been classified as DESERT, as it appears it should have been. Apparently, before adopting the Olson World Ecosystem (Olson 1992) surface types at 1/6 deg equal-angle, actual viewed grid surfaces should be checked against radiometric classifiers, such as NDVI, to ensure that their categorization is consistent with remote sensing data.

The daytime imagery (not shown) for the same geographic location as Fig.7 at night has higher land temperatures and also does not contain the low clouds. The outstanding feature of the daytime classification image is that the coastlines (Mediterranean, Red Sea, and waterways) and the Nile river are completely outlined by the partly cloudy classification. This type of erroneous classification results from the variability (between water and land) in reflectance and temperature that is picked up by the uniformity test. Unlike the nighttime scene, the principal water bodies are cool relative to the land. With one pixel over water and another over land, the reflectance and/or thermal differences certainly exceed the water thresholds for uniformity, and possibly the land thresholds also. This problem would be eliminated if, only pixels from the same background would be included in uniformity checks (not currently done).

Figure 9a is a nighttime cloud classification image of the southwestern and western USA, and eastern Pacific waters. The extensive low stratiform cloudiness over the eastern Pacific, which extends onshore in California, is captured extremely well by the LST test (showing the gross generic GL type with possible MIXED types). The nighttime T4 image alone (Fig.9b) is not very helpful for recognizing or verifying these extensive L clouds because of slight difference in cloud and water temperatures. However, in the northeastern land portion of the segment there is a questionable classification of low cloud (gold in color image) showing uniformly warm (dark) in the T4 image. If real, this cloud is warmer than the surrounding cloudfree background. Either there was an apparent LST land classification error (possibly a much lower Ch.3 emissivity), or a pronounced surface temperature inversion existed Alternatively there might have been CLEAR land areas in the region that were radiatively cooled to temperatures below the cloud top

temperatures in nearby areas.

Over land, especially around Nevada and southeastward, there is an extensive area mostly classified as PARTLY CLOUDY (colored light blue). The entire area is almost certainly cloudfree, having a characteristic cloudfree radiance pattern that is familiar to experienced human analysts of satellite T4 images of such regions. The erroneous automated classification of PARTLY CLOUDY results from the "uniformity" tests. The "uniformity" measure is based on the temperature difference between a GAC pixel and its 3 nearest neighbors in a scanline pair. If the measure exceeds the BTUT threshold, then a PARTLY CLOUDY classification is made. Inasmuch as there are pronounced terrain elevation (and possibly emissivity) variations on a compatible scale, it is likely that the uniformity measure exceeded the global land BTUT threshold (temporarily set to 2.6K at night). It follows that the BTUT threshold for this area should be increased to avoid this problem in the automated analysis. To corroborate this conclusion, the NCEP model profile data for 100 of the 110km equal-area grid cells in the same area were examined in terms of two variables: (1) modeled surface elevation, and (2) mean analyzed surface-layer temperature. The surface elevation mean was 1530m with a standard deviation of 510m. The mean surface-layer temperature was 288.4K with a standard deviation of 3.9K (well above the 2.6K threshold value). The correlation coefficient between variables was -0.67, large enough to indicate a significant relationship, but also indicating other surface or atmospheric thermal influences, including the possibility of cold air drainage. The standard deviations are consistent with the normal rate of change of temperature with altitude.

Figure 10 (for same area just discussed) includes subswath area frequency histograms of the variable D45 for two classes: (1) CLEAR LAND (Cloud Code 8) and (2) PARTLY CLOUDY (Cloud Code 72). The frequency distributions of D45 appear to be the same for both CLEAR and PARTLY CLOUDY. This supports the notion that the PC ensemble in the given subswath area actually is CLEAR.

Figure 11a, a nighttime scene in the vicinity of New Zealand, illustrates the gross generic cloud classifications for a region with complex oceanic cloud patterns. Fig.11b illustrates the land mask derived from the scanner and the land/sea auxillary database (both North and South Islands are captured in the orbital segment). Overall, the orbital distribution of the gross generic cloud classification on the pixel scale conforms very closely to that expected from the GAC Ch.4 temperature image (Fig.11c). The only problem area is the low (L) CLOUD (gold orange in the image) just east of New Zealand's South Island. CLEAR LAND appears purple in this image. [Waters west of New Zealand appear slightly warmer than those east of New Zealand on 9-6-89.] The "clouds" in the problem area appear warm and uniform (warmer than

some nearby cloudfree areas) in the Ch.4 image. CLEAR OCEAN just east of the northern end of South Island is supported by the distribution of T4-T5 in Fig.11d, which has a characteristic response to clouds when they are present. Relative to the land, D45 is elevated due to moisture over the water both east and west of New Zealand. Both areas differ with respect to the extensive areas of slightly cooler low clouds further east (detected by LST). Possibly some or most of the erroneous L classifications just east of New Zealand resulted from an LST threshold just a bit too high (as noted also in discussions of Figures 9 and 11).

The population fractions in Table 9 reveal the relative pixel counts for ascending and descending modes for a one day summary. During the ascending mode, the MLCA produced relatively more clear pixels as well as partly cloudy pixels, whereas there are significantly more cloudy pixels during descending modes. The larger daytime partly cloudy populations could be due in part to increased convective cloudiness over land. The larger nighttime cloudiness is probably related to the increased maritime lowlevel stratiform cloudiness.

Table 9. Orbital Pixel Class Summaries from CLAVR-2 by Population Fractions, Ascending and Descending Modes, 9-6-89

	asc	*desc*
pure clear	*0.1452*	*0.1175*
clear snow/ice	*0.0456*	*0.0485*
clear restored	*0.0205*	*0.0255*
*partly cloudy**	*0.4371*	*0.3326*
cloudy	*0.3516*	*0.4759*
total pixels	*31199539*	*30539199*

5.0 CONCLUSIONS AND PLANS

The CLAVR-2 can produce, in near real time, a multiple layer global cloud distribution in the pixel domain based on four gross generic cloud types (three opaque cloud types plus semitransparent cirrus), along with high quality cloudfree data over four identified surface types. All of the data needed for mapping on any desired grid are provided by the MLCA orbital routine. Final pixel decisions are dependent on special analyses over pixel ensembles within orbital subswath areas. Cloud classifications use all AVHRR channels, but thermal brightness temperature differences are emphasized in the cloud typing and layering procedures. The major objective of CLAVR-2 is to achieve a definitive database that provides a sound basis for derivation of meaningful optical and microphysical cloud properties (and cloudfree surface information). Double thresholds have been used extensively for cloud tests, allowing for an uncertainty not addressed with a single threshold. Perhaps the most pronounced change from CLAVR-1, in addition to individual pixel rather than 2x2 array classification, is the method for handling semitransparent cirrus (with or without lower clouds). Semitransparent cirrus thresholding includes cluster zone bounds, dependent on the temperature of the underlying opaque surface, that encompass all cirrus cloud temperatures and particle sizes over an opaque surface type (cloud or Earth's surface).

As expected for a pixel classifier, CLAVR-2 leads to more CLEAR pixels than does CLAVR-1, especially over the snow/ice covered polar regions. Pixel-scale products from the MLCA code, whereas designed for input to the global mapping algorithm, appear to be useful for regional analysis and validation studies in the format of a satellite image, or in a format of the user's choice. Coded gross generic classification images tend to preserve significant synoptic-scale features found in emittance or reflectance satellite images.

Despite the effectiveness of the MLCA algorithm, evaluation studies have indicated the desirability of minor changes in the code. For example, the solar zenith angle limitation the application of daytime tests should be extended from 84.3 deg to 86.0 deg. The reflectance ratio A2/A1 and the Ch. 1 reflectance (A1), in conjunction with the Ch.4 temperature, help define the daytime lower background for optically thin cirrus and aid the assessment of whether or not a pixel is cloud-filled. Evaluation of results clearly suggests that the LST thresholds for low cloud need to be lowered slightly, coupled with a less rapid increase of T3-T4 with increasing T4. The unique cirrus cluster zone thresholds defined in CLAVR-2 will need extended verification for suitability, especially during the daytime when using D45.

Plans for the future MLCA code include improvements in the auxillary data bases. The snow/ice database will be made available on a 5-day basis. In addition to the desert database, at 1/6 deg resolution,

the non-desert land will be separated into additional surface types; and all types will be checked for consistency with the monthly NDVI (Normalized Difference Vegetation Index). Ultimately, an elevation range database (flags) will be added to aid in cloudfree thermal analyses in mountainous terrain. In addition to these database improvements, a climatological database (from PATMOS) will introduce bimonthly averaged CLEAR brightness temperature and reflectance data, sorted by satellite zenith angle and surface type in large data blocks, directly into the MLCA algorithm. After the revised CLEAR datasets are established, a new procedure will be introduced for calculating Ch.3 albedo over the different land surfaces. When available, CLEAR T4 predictions from CLAVR-3 will be input directly into the CLAVR-2 algorithm, and will replace the climatological CLEAR T4 presently used in the absence of clear observations. Finally, the CLAVR-2 algorithm can be tested for consistency and suitability in handling variations in viewing and illumination conditions, or other remote sensing parameters, by application to two polar orbiting satellites operating at the same time (e.g., NOAA-12 & NOAA-14) to provide four views per gridcell each day.

As described in Part II of this paper, the Cloud Layered Data Set (CLDS) algorithm is a mapper routine that takes the gross generic output from the MLCA and maps the "most nadir" orbital data (in regions of overlap) into a $(110\ km)^2$ equal-area grid over the globe (separately for ascending and descending modes). Statistics are formed for each pixel classification within each grid cell. An elaborate cloud amount procedure is followed to determine the fractional cloud amount contribution by each PARTLY CLOUDY ensemble to the total cloud amount of each gross generic type. The gross generic opaque types in a grid cell can be subdivided into separate cloud layers if the frequency distributions so indicate. Finally, all pertinent radiance statistics are summarized for each CLOUD and CLEAR ensemble in the grid cell, and pertinent NCEP temperature-moisture height profiles are added to the dataset for each grid cell. With the aid of these soundings, it is possible to perform a wide variety of analyses on the data, including retrieval of both physical and optical cloud properties. Instantaneous flux distributions can be calculated from the data and radiative forcing on the atmospheric energetics can be assessed.

7.0 APPENDIX

Brightness Temperature and Emissivity

Tests involving Ch.3 in particular must deal with interchannel changes in spectral emissivity associated with the background surface. Computational simulation of the impact of stipulated Ch.3 changes in background surface emissivity on brightness temperature differences requires familiarity with the two-way conversions between measured radiance and brightness temperature.

The monochromatic Planck function specifically defines Planckian (blackbody) spectral radiance $B_\nu(T_B)$ in terms of the brightness temperature T_B at the particular wavenumber (or wavelength). The filtered radiance measured by an AVHRR channel with a specific spectral response function Φ_ν (normalized to its maximum) can be represented as an equivalent spectral radiance $R_\nu(T_B)$ for each channel through

$$R_\nu(T_B) = \int B_\nu(T_B)\, \Phi_\nu \, d\nu \,/\, \int \Phi_\nu \, d\nu \qquad \text{(A1)}$$

where the denominator is the equivalent width in wavenumber. By inserting all possible temperatures in the generation of B_ν, a complete detailed table of T_B and the corresponding spectral radiance R_ν is obtained from A1. Such a table is ideal for converting from temperature to radiance when the temperature is used as an index for direct table look-up.

As an alternative to the table, the Planck equation can be used to relate R_ν and T_B, provided that a suitable wavenumber can be defined to allow replacement of B_ν with R_ν in the Planck equation. However, the effective wavenumber (or so-called central wavenumber) to go along with the given T_B would be a temperature-dependent variable. The most precise, efficient, and rapidly-applied relationship uses instead the constant centroid wavenumber, ν_C, which is the wavenumber that equally divides the equivalent width. When the temperature-independent centroid wavenumber is used in the Planck equation, precise agreement (better than 0.1%) with the tabular values can be obtained if brightness temperature is replaced with an effective brightness temperature, T_E, which is a linear function of T_B and very close in magnitude:

$$T_E = a_i + b_i T_B \qquad \text{(A2)}$$

where the subscript i on the offset and slope coefficients is to identify the AVHRR channel. Constants a_i, b_i, and ν_C are listed in Table A1 for each thermal channel of each satellite with a five-channel AVHRR instrument. The distinction between T_E and T_B appears to be significant only for AVHRR Ch.3.

Either R_ν, in units mW m^{-2} sr^{-1} $(cm^{-1})^{-1}$, or T_B, in units deg K, can be determined from

$$R_\nu(T_B) = C_1 \nu_C^{\,3} / \{\mathrm{EXP}[C_2 \nu_C / T_E] - 1\} \qquad \text{(A3)}$$

or

$$T_E = a_i + b_i T_B = C_2 \nu_C / \mathrm{LN}[\{C_1 \nu_C^{\,3} / B(T_B)\} + 1] \qquad \text{(A4)}$$

where C_1 = 1.191066E-05 and C_2 = 1.438833. If the emissivity e, where e < 1 for Ch. 3, is introduced, and the subscript ν is dropped from the spectral radiance, then

$$R(T_B) = e\, B(T_N), \text{ where } T_N > T_B. \qquad (A5)$$

The actual emission temperature T_N must exceed the brightness temperature T_B for all e less than unity. Also,

$$\{C_1 \nu_C^3 / B(T_B)\} = (1/e)\{C_1 \nu_C^3 / B(T_N)\} \qquad (A6a)$$

$$\{C_1 \nu_C^3 / B(T_N)\} = e\,\{C_1 \nu_C^3 / B(T_B)\}\ . \qquad (A6b)$$

From these expressions, brightness temperature (or the effective brightness temperature) can be related to the actual emission temperature (or effective emission temperature):

$$T_E = a_i + b_i T_B = C_2 \nu_C / \mathrm{LN}[(1/e)\{\mathrm{EXP}(C_2 \nu_C / T_N') - 1\} + 1] \qquad (A7)$$

where $T_N' = a_i + b_i T_N$.

These expressions have been used extensively to simulate the impact of specified emissivity and associated emission temperatures, especially for Ch.3, on brightness temperature near the surface. Simulations are extended to estimate satellite-measured cloudfree brightness temperature differences, such as D34 and D35. The thermal channel centroid wavenumbers and linear coefficients described above are given in Table A1 for the AVHRR instrument on each NOAA Polar Orbiting Satellite.

Table A1. AVHRR Thermal Channel Centroid Wavenumbers (WNO) and Linear Coefficients Relating Effective Brightness Temperature T_E to Observed Brightness Temperature T_B [$T_E = a_i + b_i T_B$]

INSTRUMENT		WNO	a_i	b_i
NOAA-07	CH.3	2682.37	1.90454	.996627
	CH.4	927.350	0.39560	.998716
	CH.5	840.181	0.20594	.999121
NOAA-09	CH.3	2688.07	1.84003	.996667
	CH.4	929.571	0.37351	.998765
	CH.5	844.990	0.25558	.999077
NOAA-11	CH.3	2680.05	1.73316	.996657
	CH.4	927.462	0.32081	.998788
	CH.5	840.746	0.04862	.999336
NOAA-12	CH.3	2648.64	1.83043	.996334
	CH.4	920.524	0.34654	.998586
	CH.5	836.497	0.13486	.999235
NOAA-14	CH.3	2654.25	1.87812	.996176
	CH.4	928.349	0.30794	.998559
	CH.5	833.040	-0.02216	.999462

Table A2. Cloud Test Threshold Tables (T4: CIRT1; CIRT2; FMFT1; FMFT2; LSTOCN; ULST/OCN (CLAVR1); LSTH2 (270-295K)

T4	CIRT1	CIRT2	FMFT1	FMFT2	LSTOCN	ULST35	LSTH2
	T3-T5	T3-T5	T4-T5	T4-T5	T3-T4	T3-T5	T3-T4
240	1.500	2.500	0.000	0.200	-0.350	-0.690	
241	1.500	2.500	0.000	0.200	-0.350	-0.679	
242	1.500	2.510	0.000	0.210	-0.350	-0.668	
243	1.500	2.540	0.000	0.240	-0.350	-0.656	
244	1.500	2.570	0.000	0.270	-0.350	-0.644	
245	1.500	2.600	0.000	0.300	-0.350	-0.632	
246	1.520	2.640	0.000	0.330	-0.350	-0.619	
247	1.540	2.700	0.000	0.360	-0.350	-0.605	
248	1.560	2.780	0.000	0.390	-0.350	-0.592	
249	1.580	2.860	0.000	0.420	-0.350	-0.578	
250	1.600	2.950	0.000	0.460	-0.350	-0.563	
251	1.620	3.050	0.000	0.500	-0.348	-0.548	
252	1.640	3.150	0.010	0.550	-0.346	-0.532	
253	1.660	3.250	0.020	0.600	-0.344	-0.516	
254	1.680	3.350	0.030	0.650	-0.342	-0.499	
255	1.700	3.450	0.040	0.710	-0.340	-0.481	
256	1.730	3.560	0.050	0.770	-0.338	-0.463	
257	1.760	3.680	0.060	0.830	-0.336	-0.444	
258	1.790	3.810	0.070	0.890	-0.334	-0.425	
259	1.820	3.920	0.080	0.950	-0.332	-0.405	
260	1.850	4.050	0.100	1.020	-0.330	-0.384	
261	1.900	4.190	0.120	1.100	-0.328	-0.363	
262	1.950	4.350	0.140	1.180	-0.326	-0.341	
263	2.000	4.540	0.160	1.260	-0.324	-0.318	
264	2.050	4.770	0.180	1.350	-0.322	-0.294	
265	2.100	5.050	0.200	1.440	-0.320	-0.269	
266	2.170	5.340	0.220	1.540	-0.317	-0.244	
267	2.250	5.640	0.240	1.640	-0.313	-0.218	
268	2.330	5.950	0.260	1.740	-0.309	-0.190	
269	2.410	6.270	0.290	1.840	-0.305	-0.162	
270	2.500	6.600	0.320	1.950	-0.300	-0.133	0.000
271	2.650	6.970	0.360	2.070	-0.295	-0.103	0.000
272	2.820	7.390	0.400	2.200	-0.290	-0.072	0.050
273	2.990	7.850	0.440	2.340	-0.285	-0.039	0.010
274	3.160	8.350	0.490	2.490	-0.280	-0.006	0.015
275	3.350	8.900	0.540	2.640	-0.275	0.029	0.020
276	3.600	9.500	0.600	2.800	-0.269	0.064	0.025
277	3.870	10.150	0.680	2.960	-0.263	0.101	0.030
278	4.160	10.850	0.780	3.130	-0.257	0.140	0.035
279	4.470	11.600	0.880	3.300	-0.251	0.179	0.040
280	4.800	12.400	1.000	3.470	-0.245	0.220	0.048

281	5.180	13.320	1.130	3.650	-0.238	0.263	0.065
282	5.620	14.420	1.260	3.840	-0.229	0.307	0.082
283	6.160	15.540	1.400	4.030	-0.220	0.352	0.099
284	6.820	16.700	1.550	4.230	-0.210	0.399	0.116
285	7.600	17.850	1.700	4.430	-0.200	0.448	0.133
286	8.460	18.980	1.890	4.650	-0.188	0.499	0.150
287	9.360	20.100	2.100	4.880	-0.176	0.551	0.167
288	10.320	21.200	2.330	5.120	-0.164	0.605	0.184
289	11.360	22.300	2.580	5.370	-0.152	0.661	0.202
290	12.500	23.350	2.850	5.620	-0.140	0.718	0.220
291	13.710	24.300	3.130	5.880	-0.126	0.778	0.238
292	14.980	25.150	3.410	6.150	-0.109	0.840	0.256
293	16.270	26.000	3.690	6.430	-0.089	0.904	0.274
294	17.500	26.800	3.970	6.720	-0.066	0.970	0.292
295	18.650	27.600	4.250	7.020	-0.040	1.039	0.310
296	19.710	28.300	4.650	7.330	-0.010	1.110	0.328
297	20.710	28.800	5.050	7.640	0.028	1.183	0.346
298	21.650	29.200	5.450	7.960	0.074	1.259	0.364
299	22.510	29.600	5.850	8.270	0.126	1.338	0.382
300	23.250	30.000	6.250	8.570	0.180	1.419	0.400
301	23.800	30.300	6.600	8.860	0.235	1.503	0.418
302	24.250	30.600	6.900	9.150	0.290	1.590	0.436
303	24.600	30.700	7.200	9.440	0.345	1.680	0.454
304	24.850	30.750	7.500	9.720	0.400	1.774	0.472
305	25.000	30.800	7.800	10.000	0.455	1.870	0.490
306	25.000	30.800	7.800	10.000	0.510	1.970	
307	25.000	30.800	7.800	10.000	0.565	2.073	
308	25.000	30.800	7.800	10.000	0.620	2.180	
309	25.000	30.800	7.800	10.000	0.675	2.291	
310	25.000	30.800	7.800	10.000	0.730	2.406	
311	25.000	30.800	7.800	10.000	0.785	2.524	
312	25.000	30.800	7.800	10.000	0.840	2.647	
313	25.000	30.800	7.800	10.000	0.895	2.773	
314	25.000	30.800	7.800	10.000	0.950	2.905	
315	25.000	30.800	7.800	10.000	1.005	3.041	
316	25.000	30.800	7.800	10.000	1.060	3.181	
317	25.000	30.800	7.800	10.000	1.115	3.327	
318	25.000	30.800	7.800	10.000	1.170	3.477	
319	25.000	30.800	7.800	10.000	1.225	3.633	
320	25.000	30.800	7.800	10.000	1.280	3.794	

* LSTLND = LSTOCN - 2; LSTDES = LSTOCN - 4

**A secondary threshold (LSTH2) for checking the presence of PARTLY CLOUDY conditions from BTD T3-T4 over the ocean is given by the last column in the table for the T4 range from 270K to 295K.

Description of Pixel Classification Process in MLCA

This Appendix describes the sequential order of the pixel tests in MLCA. The LST(D34), CIRT(D35), and FMFT(D45) thresholds currently included in the MLCA algorithm are listed in Table A2. BTD thresholds described here are based on extensive simulations, as they were in CLAVR-1, whereas other thresholds are empirically defined in terms of climatological clear sky values. These thresholds are updated during the subswath area analysis. Brief discussion of the flow charts are given below. Though not every detail in the flowcharts is explained, the following discussions attempt to illustrate the main points and logical and sequential structure of MLCA night and day algorithms. In the following discussion, a passing of a test indicates that condition for a cloudy pixel was met.

- **Nighttime Pixel Classification**

Table 3 in Section 3.2 has listed the key initial tests sequentially and the entire sequential decision process for the nighttime pixel classification is shown in Fig. A1. In the first sequence of tests, GOCT, uses the D45 thresholds THH and THG which are computed as functions of the clear sky T4. If D45 exceeds THH is the pixel is classified as cirrus (H) and if D45 lies between THH and THG, the pixel is classified as opague glaciated cloud (G). For pixels with latitudes greater than 67 ^{o} and classified as being over ice, a spatial nonuniformity test (CTUT) is applied to the values of DT4. If DT4 passes CTUT, the pixel is classified as partly covered by opaque clouds (PC-0), otherwise is it classified as clear snow/ice. If the pixel were not over ice, it would be classified as G. If the pixel fails the GOCT, the LST test is applied next. If this test is passed and T4 < 294 K, the pixel is classified as liquid opaque cloud (L). Also shown is a condition that if T5 > 315 K, a cloud classification is not made.

Pixels failing the LST move on down to the third group of tests to attempt to classify semitransparent cirrus alone or over other opaque cloud types. First, a check of A1 is performed. If A1 registers a sufficient amount of solar energy, the semitransparent tests described in Section 2.2 are used otherwise the night procedure described in Section 2.3 is used. The resulting classifications are either semitransparent cirrus (H) or are assigned an intermediate classification until the subswath area analysis (Section 3.4) which will allow for identification of cirrus over opaque cloud types.

If a pixel is not classified as semitransparent cirrus, the tests in the fourth group are applied. A pixel is first subjected to the FMFT. If this test is passed and T4 < 263 K, the pixel is classified as mixed phase (M). If T4 > 263 K, but the pixel passes CTUT, the pixel is not finally classified until the subswath area analysis since

they are probably mixtures of yet unidentified opaque types. Pixels which fail FMFT and are known not to be over snow/ice or land are subjected to the BTUT. If the BTUT is passed, the pixel is classified as partly cloudy opaque (PC-O).

The final tests attempt to classify remaining pixels as clear and to subclassify the clear pixels with snow/ice and land/sea tests. A final classification of partly cloudy liquid cloud (L) is possible for pixels over water which have D34 above the LSTOCN threshold but fall below the LSTH2 thresholds. The differing LST thresholds are described in Section 2.4.

- **Daytime Pixel Classification Flowchart**

Table 4 in Section 3.3 listed the key initial daytime test sequences that appear in the flowchart in Fig A2. Unlike CLAVR-1, CLAVR-2 uses the same initial thermal (GOCT) in both day and night algorithms. As in the night algorithm, the day algorithm can be broken down into five sequential groups with similar functions as in the nighttime algorithm. The major change in the thermal tests from night to day is the daytime application of FMFTH (instead of CIRT) to define semitransparent cirrus. The nightime LST thermal test is dropped as well as CIRT.

A pixel failing GOCT is now subjected to the FMFTH test. A pixel with D45 exceeding the FMFT1 threshold, is then subjected to a procedure outlined in Section 2.3. If D45 is less then FMFT2, a PC-H determination is made or the classification is made in a series of tests labeled "A" in the flowchart. If D45 exceeds FMFT2, a final cirrus classification is deferred until the subswath analysis. The A1CT and A2/A1 tests also make use of the subroutine "A", which also includes A1 and A2/A1 tests internally. Classification of PC-O, PC-L, L, and M come from "A". Both the A1CT and A2/A1 sequence include checks for sun glint over water.

Pixels failing the A2/A1 test are then subjected to the background nonuniformity tests. Pixels passing BTUT and BRUT are classified as PC-O. Pixels failing BTUT and BRUT (radiatively uniform) are classified as clear with the clear subclassification depending on the snow/ice and land/sea tests.

REFERENCES

Arking, A., and J.D. Childs, 1985: Retrieval of cloud cover parameters from multispectral satellite images. J. Climate & Appl. Meteor., 24, 322-333.

Baum, B.A., R.F. Arduini, B.A. Wielicki, P. Minnis and S-C Tsay, 1994: Multilevel Cloud Retrieval Using Multispectral HIRS and AVHRR Data: Nighttime Oceanic Analysis. J. Geophys. Res., 99, 5499-5514.

Baum, B.A., T. Uttal, M. Poellot, T.P. Ackerman, J.M. Alvarez, J. Intieri, D. O'C. Starr, J. Titlow, Y. Tovinkere, and E. Clothiaux, 1995: Satellite Remote Sensing of Multiple Cloud Layers. J.Atmos. Sci., 52, 4210-4230.

Chou, M.D., J. Childs, and P. Dorian, 1986: Cloud cover estimation using bispectral satellite measurements. J. Climate & Appl. Meteor., 25, 1280-1292.

Coakley, J.A. amd F.P. Bretherton, 1982: Cloud cover from high resolution scanner data: detecting and allowing for partially filled fields of view. J. Geophys. Res., 87, 4917-4932.

Coll, C., V. Caselles, and T.J. Schmugge, 1994: Evaluation of Land Surface Emissivity Differences in the Split-Window Channels of AVHRR. Remote Sens. Evniron., 48, 127-134.

Davis, P.A., 1993: Spectral Radiance-Temperature Conversions for Measurements by AVHRR Thermal Channels 3,4,5. NOAA Technical Report NESDIS 71, U.S. Dept. of Commerce, Washington, DC, 51pp.

Dozier, J., and S.G. Warren, 1982: Effect of Viewing Angle on the Infrared Brightness Temperature of Snow. Water Resources Research, 18(5), 1424-1434.

d'Entremont, R.P.,1986: Low and Mid-level Cloud Analysis Using Nighttime Multispectral Imagery. J. Climate Appl. Meteor.,25,
1853-1869.

Francois, C. and C. Ottle,1994: Estimation of the Angular Variation of the Sea Surface Emissivity with the ASTIR/ERS-1 Data. Remote Sensing of the Environment, 48, (3), 302-308.

Giraud, V., J.C. Buriez, Y. Fouquart, F. Parol, and G. Seze, 1996: Large-Scale Analysis of Cirrus Clouds from AVHRR Data: Assessment of Both a Microphysical Index and the Cloud-Top Temperature. J. Appl. Meteor., 36, 664-675.

Hamill, T.M., R.P. d'Entremont, and J.T. Bunting, 1992: A description of the Air Force real time nephanalysis model. Weather Forecasting, 7, 288-306.

Inoue, T.,1985: On the temperature and effective emissivity determination of semi-transparent cirrus clouds by bispectral measurements in the 10 µm window region. J. Meteor. Soc. Japan, 63,
88-98.
------, 1987: A cloud type classification with NOAA-7 split-window measurements. J. Geophys. Res., 92, 3991-4000.

Luo, G., X. Lin and J.A. Coakley, Jr., 1994: 11-µm Emissivities and Droplet Radii for Marine Stratocumulus. J. Geophys. Res., 99, 3685-3698.

Luo, G., P.A. Davis, L.L. Stowe, and E.P. McClain, 1995: A Pixel-Scale Algorithm of Cloud Type, Layer, and Amount for AVHRR Data. Part I: Nighttime. J. Atmos. Ocean. Tech., 12, 1013-1037.

Luo, G., L.L. Stowe, and P.A. Davis, 1997: An Intercomparison of Total and Layered Cloud Amount Between CLAVR, ISCCP, and MSMR for the November 28,1991 FIR-II Region. Submitted to J.Atmos. and Oceanic Tech.

Minnis,P., K.N. Liou, and Y. Takano, 1993: Inference of cirrus cloud properties using satellite observed visible and infrared radiances. Part I Parameterization of radiance fields. J. Atmos. Sci., 50, 1279-1304.

Olson, J.S.,1992: World Ecosystems (WE1.4d): Digital Data in Global Change Data Base, Digital Data with Documentation, NOAA, National Geophysical Data Center, Boulder, CO, pp.A5-1 to A5-36.

Ou, S.C., K.N. Liou, and B.A. Baum, 1996: Detection of Multilayer Cirrus Cloud Systems Using AVHRR Data: Verification Based on FIRE II IFO Composite Measurements. J. Appl.Meteor., 35, 178-191.

Rossow, W.B., and L.C. Gardner, 1993: Cloud detection using satellite measurements of infrared and visible radiances for ISCCP. J. Climate, 6, 2341-2369.

----------, ----------, 1993: Validation of ISCCP and other cloud amounts. J. Climate, 6, 2370-2393.

Rossow, W.B., A.W. Walker, and L.C. Gardner, 1993: Comparison of ISCCP and other cloud amounts. J. Climate, 6, 2394-2418.

Salisbury, J.W., and D.M. D'Aria, 1994: Emissivity of Terrestrial Materials in the 3-5 μm Atmospheric Window. Remote Sens. Environ., 47, 345-361.

Saunders, R.W. and K.T. Kriebel, 1988: An improved method for detecting clear sky and cloudy radiances from AVHRR data. Int. J. Remote Sensing, 9, 123-150.

Stowe, L.L., H.Y.M. Yeh, C.G. Wellemeyer, H.L. Kyle, & the Nimbus-7 Cloud Data Processing Team, 1989: Nimbus-7 Global Cloud Climatology, Part II: First year results. J. of Climate,2, 671-709.

Stowe, L.L., E.P. McClain, R. Carey, P. Pellegrino, G.Gutman, P. Davis, C. Long, and S. Hart, 1991: Global Distribution of Cloud Cover derived from NOAA/AVHRR Operational Satellite Data. Adv Space Res., 11, 51-54.

Stowe, L.L., S.K. Vemury, and A.V. Rao, 1993: AVHRR Clear-Sky Radiation Data Sets at NOAA/NESDIS. Adv. Space Res.,14,(1)113-116.

Stowe, L.L., P.A. Davis, and E.P. McClain, 1997: Global Cloud Cover from NOAA/AVHRR Data: Scientific Basis and Evaluation of the CLAVR-1 Classification Algorithm. J. Atmos. Ocean. Tech. (submitted).

Stowe, L.L. and H.Jacobowitz, 1997: The AVHRR Pathfinder Atmosphere

Project. Proceedings, AMS Annual Meeting, Feb. 1997, Long Beach,CA

Stubenrauch, C.J., N.A. Scott, and A. Chedin, 1996: Cloud Field Identification for Earth Radiation Budget Studies. Part I: Cloud Field Classification Using HIRS-MSU Sounder Measurements. J. Appl. Meteor.,35, 416-427.

Takano,Y. and K.N. Liou,1989: Radiative transfer in cirrus clouds. I. Single scattering and optical properties of oriented hexagonal ice crystals. J. Atmos. Sci.,46, 3-20.

Wielicki, B.A., B.R. Barkstrom, E.D. Harrison, R.B. Lee, III, G.L. Smith, and J.E. Cooper, 1996: Clouds and the Earth's Radiant Energy System (CERES): An Earth Observing System Experiment. Bull. Amer. Meteor. Soc., 77(5), 853-868.

Wylie, D.P., W.P. Menzel, H.M. Woolf, and K.I. Strabala, 1994: Four Years of Global Cirrus Cloud Statistics Using HIRS. Jour. Clim.,7, 1972-1986.

TABLES

Table 1. Radiometric (Thermal) Generic Cloud Types

Table 2. Sequential Procedures in MLCA Pixel Processor

Table 3. Nighttime Cloud Test Sequence

Table 4. Daytime Cloud Test Sequence

Table 5. Ch.3 Temperature Adjustment(DT3) for Surface Reflectance

Table 6. Codes for MIXED Cloud Types

Table 7. MLCA Semitransparent Cirrus Cloud Codes

Table 8. Color Image Plan for MLCA Gross Generic Cloud Codes

Table 9. Orbital Pixel Class Summaries from CLAVR-2 by Fractions of Total Populations for Ascending and Descending Modes, September 6, 1989

Table A1. AVHRR Thermal Channel Centroid Wavenumbers (WNO) and Linear Coefficients Relating Effective Brightness Temperature T_E to Observed Brightness Temperature T_B [$T_E = a_i + b_i T_B$]

Table A2. Cloud Test Threshold Tables (T4: CIRT1; CIRT2; FMFT1; FMFT2; LSTOCN; ULST/OCN (CLAVR1); LSTH2 (270-295K)

ILLUSTRATIONS

Figure 1. Simulated (T4,T3-T5) Nighttime Semitransparent Cirrus Pixels for Two Cloud Temperatures a) Midlatitude Summer Temperature-Moisture Profile b) Midlatitude Winter Temperature-Moisture Profile

Figure 2.Nighttime Semitransparent Cirrus Lateral Cluster Zone Bounds Containing Pixels Associated with Midlatitude Summer and Winter Profiles and Surface Temperatures (BTD=T3-T5)

Figure 3. Daytime Semitransparent Cirrus Lateral Cluster Zone Bounds Containing Pixels Associated with Midlatitude Summer and Winter Profiles and Surface Temperatures (BTD=T4-T5)

Figure 4. Nighttime Low (Liquid) Stratiform Test Thresholds CLAVR-2, T3 - T4: OCEAN, LAND, DESERT; CLAVR-1, T3-T5: OCEAN

Figure 5. Daytime Scene, South Central USA, Orbit 489899, 9-6-89 (a) Gross Generic Cloud Types (b) NOAA-11 T4 (c) A2

Figure 6. Scattergrams of Daytime D45 Semitransparent Cirrus Classifications a) D45 & T4 b) Reflectance A1 & T4 c) A2/A1 & T4

Figure 7. Night Scene, Egypt-Saudi Arabia, Orbit 490102, 9-6-89 (a) Gross Generic Cloud Classes (b) T4

Figure 8. Scattergrams of T3-T4 (ULST) for Low Cloud and Clear Pixels Over Desert and Nondesert Land (Fig.7)

Figure 9. AVHRR GAC CH.4 Temperature and CLAVR-2 Gross Generic Cloud Classifications, Western USA and E.Pacific Coast, Orbit 489394, Nighttime, 9-6-89

Figure 10. Nighttime Frequency Distributions of T4-T5 for Clear and Partly Cloudy Classes, Western USA, 9-6-89 (a) CLEAR T4-T5 (b) PTLY CLDY T4-T5

Figure 11. AVHRR GAC CH.4 Temperature and CLAVR-2 Gross Generic Cloud Classifications, New Zealand Area, Orbit 489596, Nighttime, 9-6-89

Figure A1. Nighttime Pixel Classification Flowchart

Figure A2. Daytime Pixel Classification Flowchart

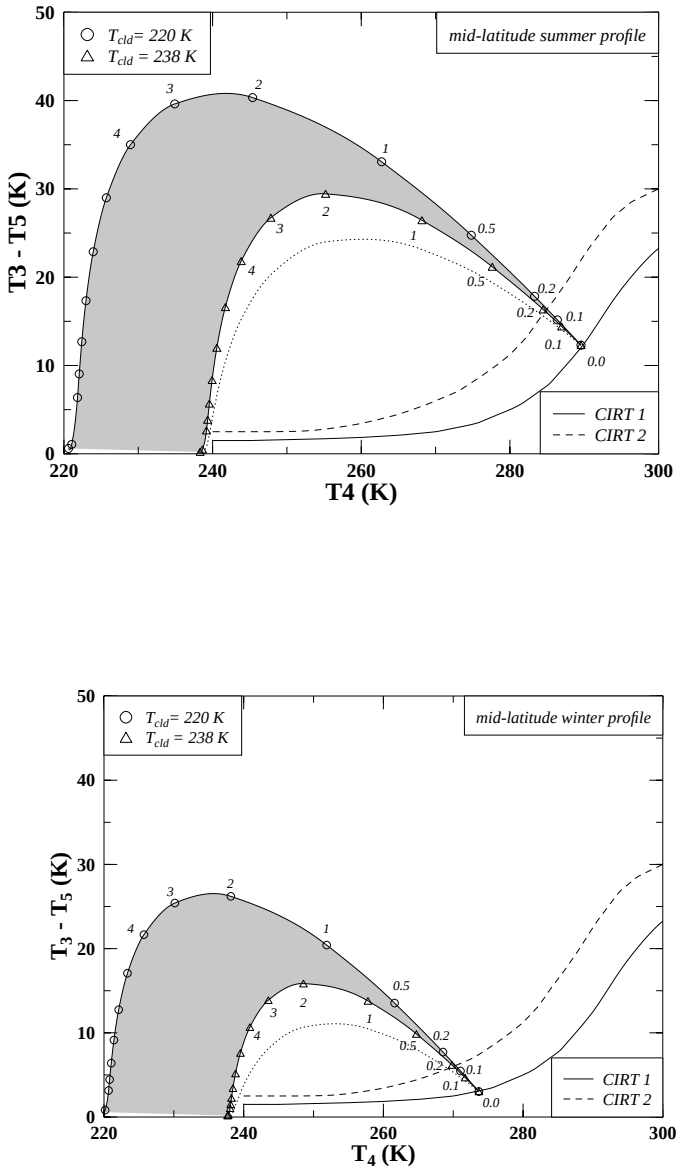

Figure 1. Simulated (T4,T3-T5) Nighttime Semitransparent Cirrus Pixels for Two Cloud Temperatures a) Midlatitude Summer Temperature-Moisture Profile b) Midlatitude Winter Temperature-Moisture Profile

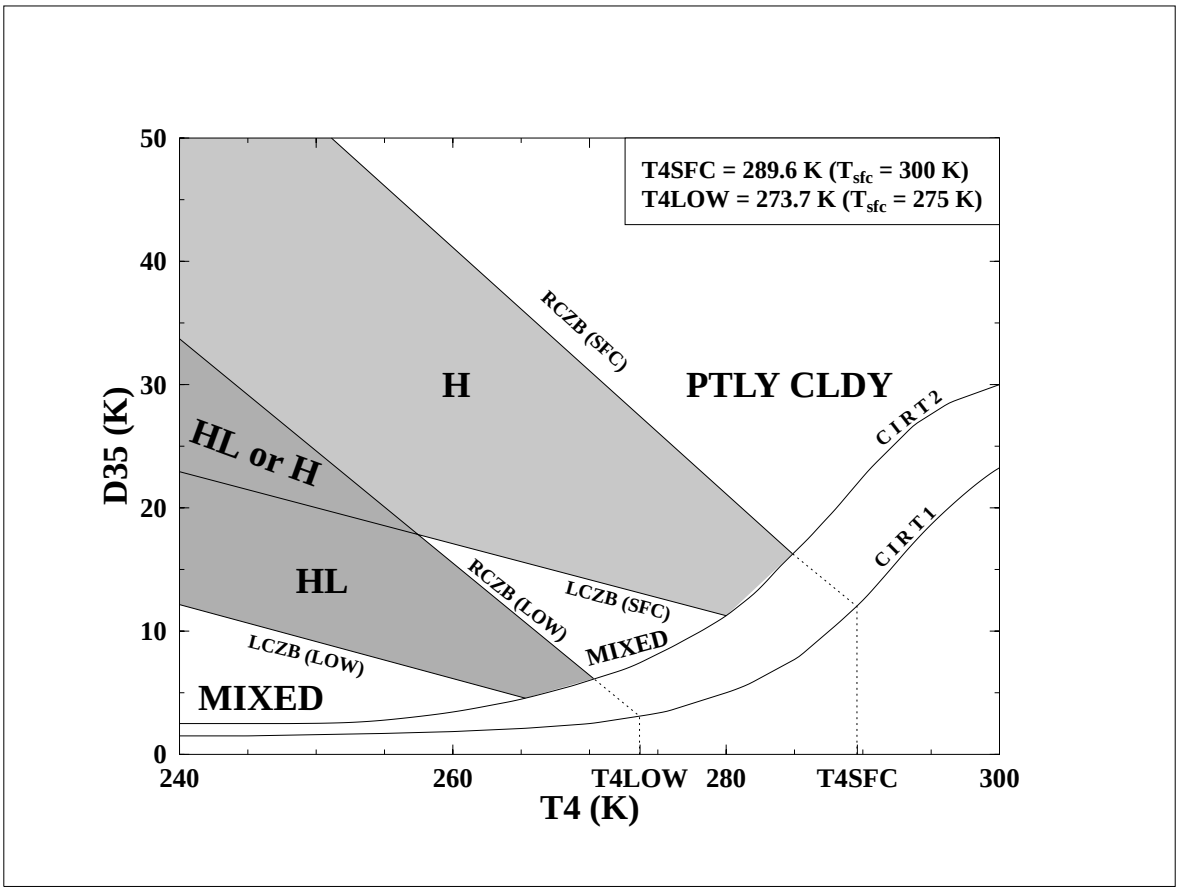

Figure 2.Nighttime Semitransparent Cirrus Lateral Cluster Zone Bounds Containing Pixels Associated with Midlatitude Summer and Winter Profiles and Surface Temperatures.

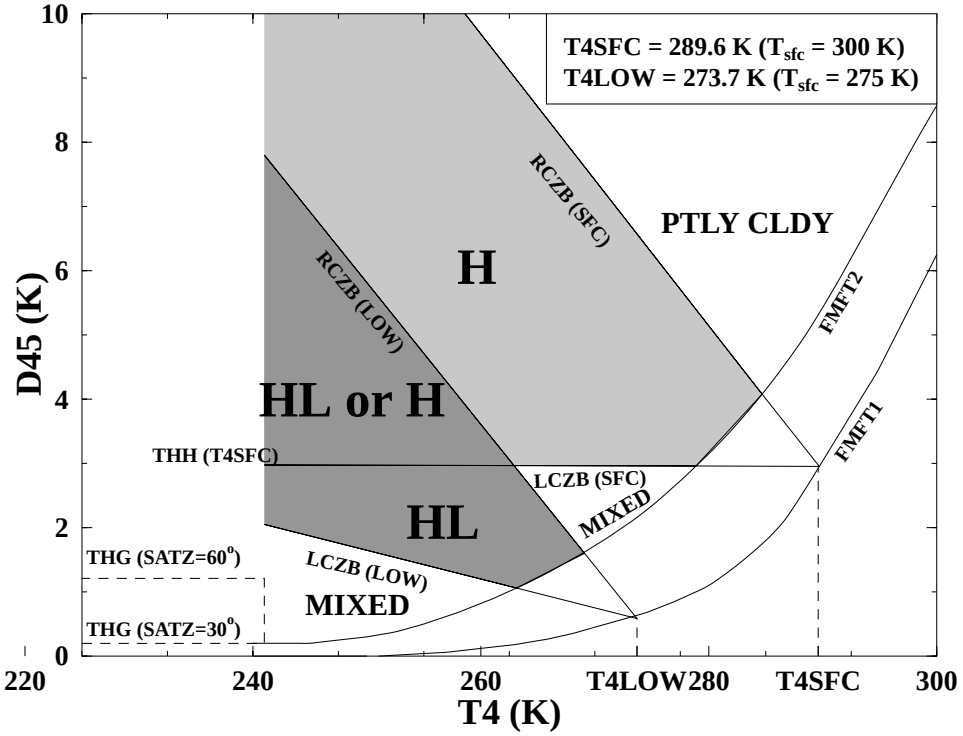

Figure 3. Daytime Semitransparent Cirrus Lateral Cluster Zone Bounds Containing Pixels Associated with Midlatitude Summer and Winter Profiles and Surface Temperatures.

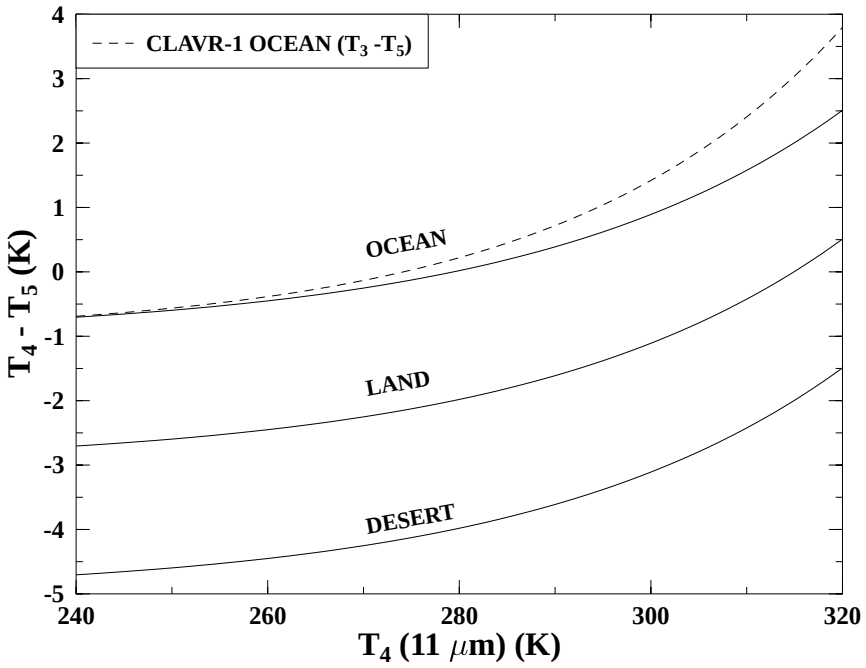

Figure 4. Nighttime Low (Liquid) Stratiform Test Thresholds CLAVR-2, T3 - T4: OCEAN, LAND, DESERT; CLAVR-1, T3-T5: OCEAN

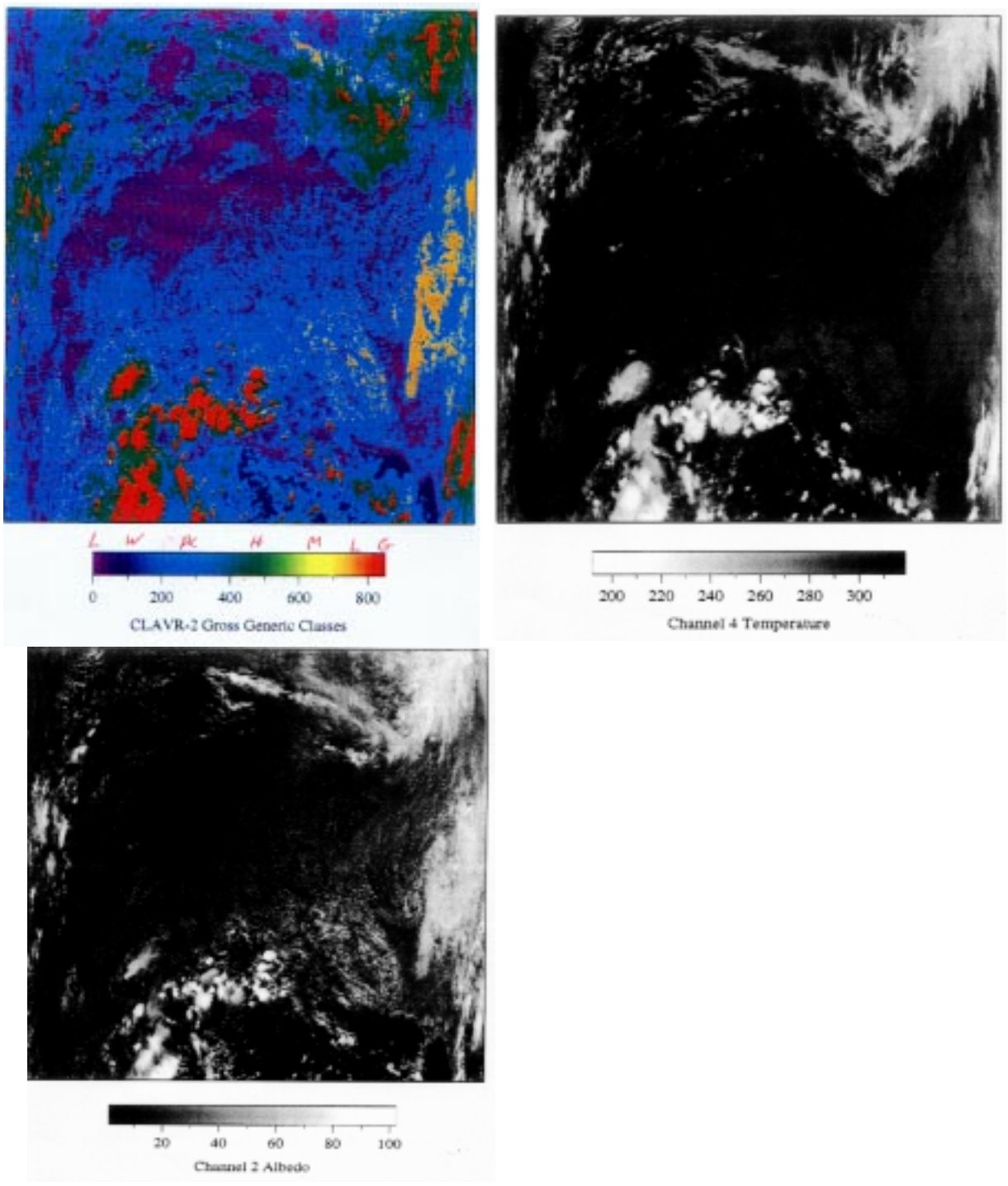

Figure 5. Daytime Scene, South Central USA, Orbit 489899, 9-6-89 (a) Gross Generic Cloud Types (b) NOAA-11 T4 (c) A2

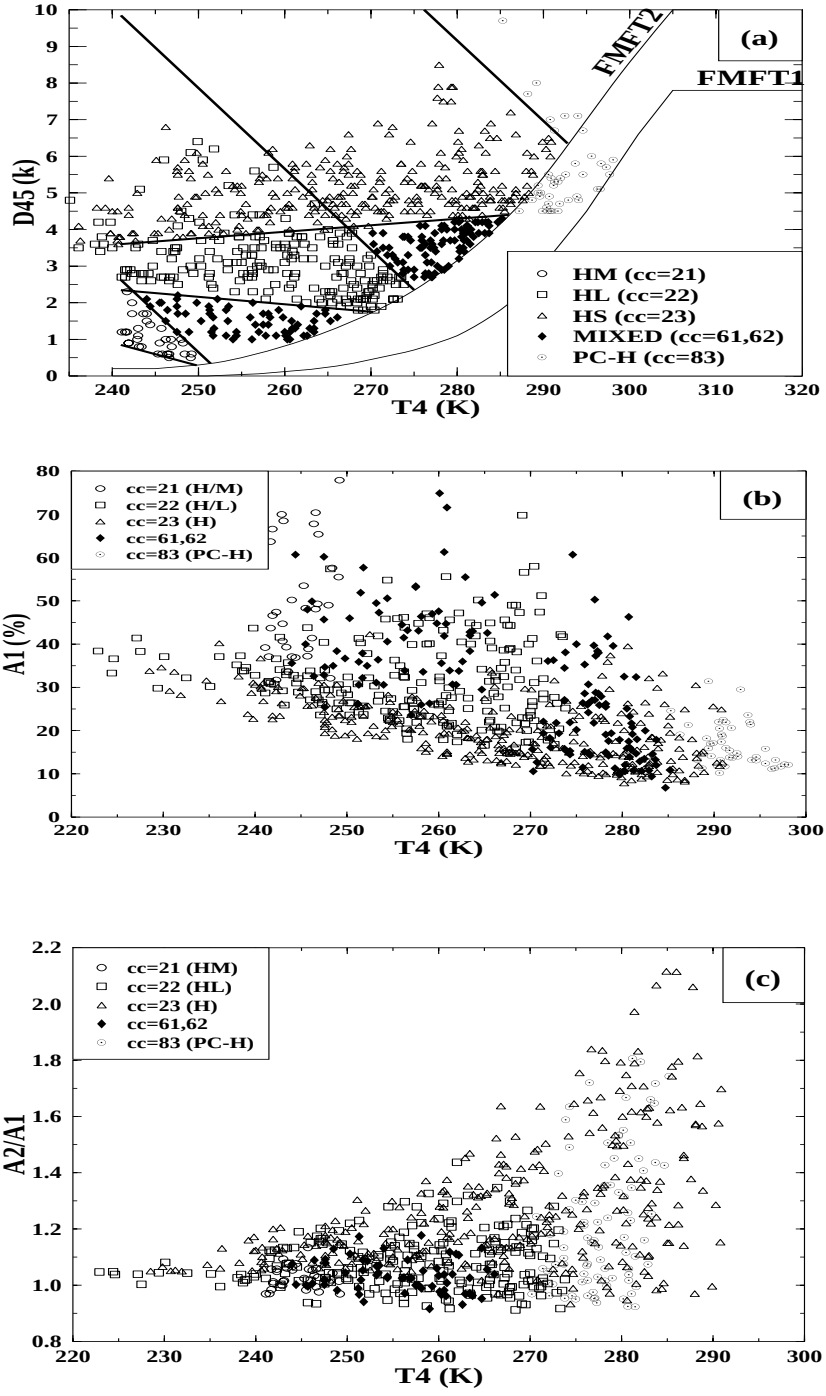

Figure 6. Scattergrams of Daytime D45 Semitransparent Cirrus Classifications a) D45 & T4 b) Reflectance A1 & T4 c) A2/A1 & T4.

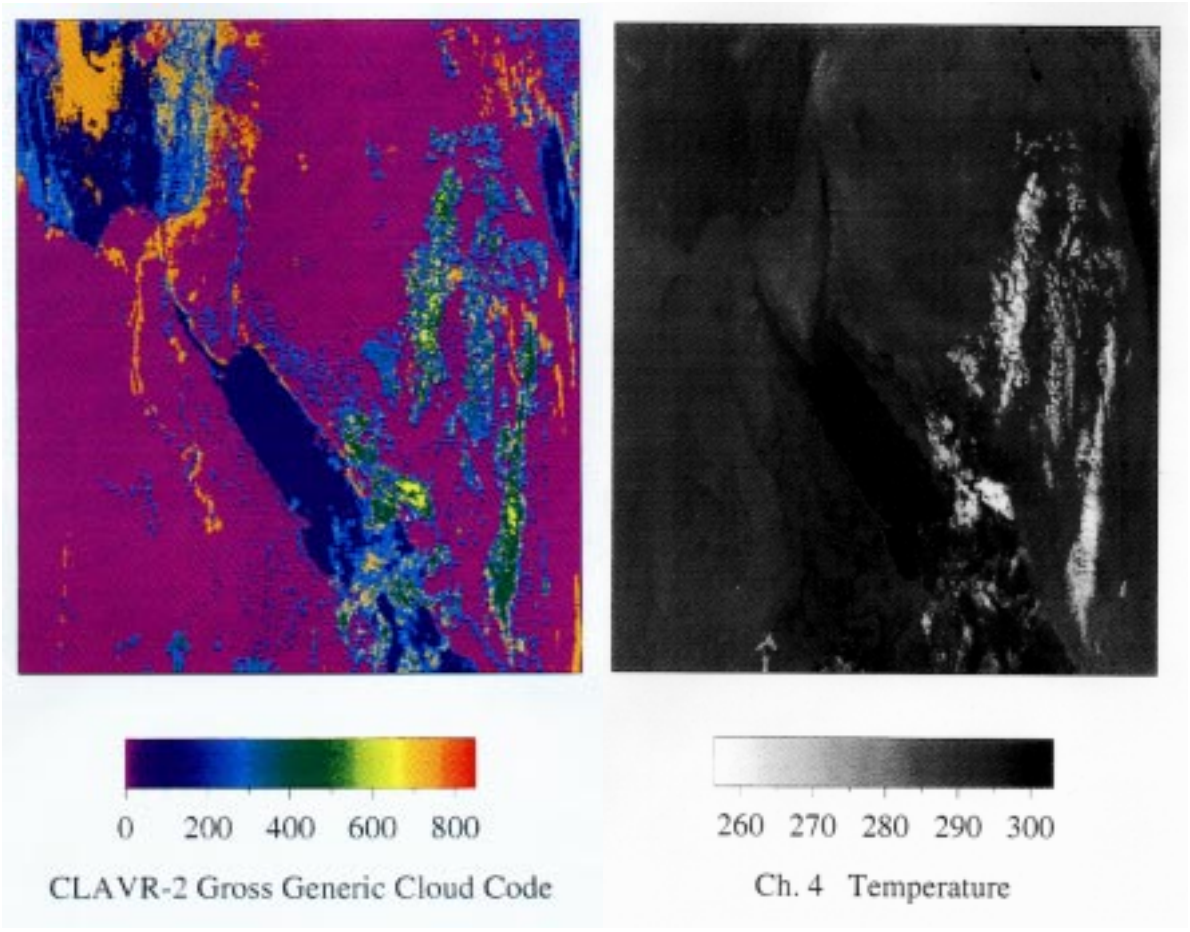

Figure 7. Night Scene, Egypt-Saudi Arabia, Orbit 490102, 9-6-89 (a) Gross Generic Cloud Classes (b) T4

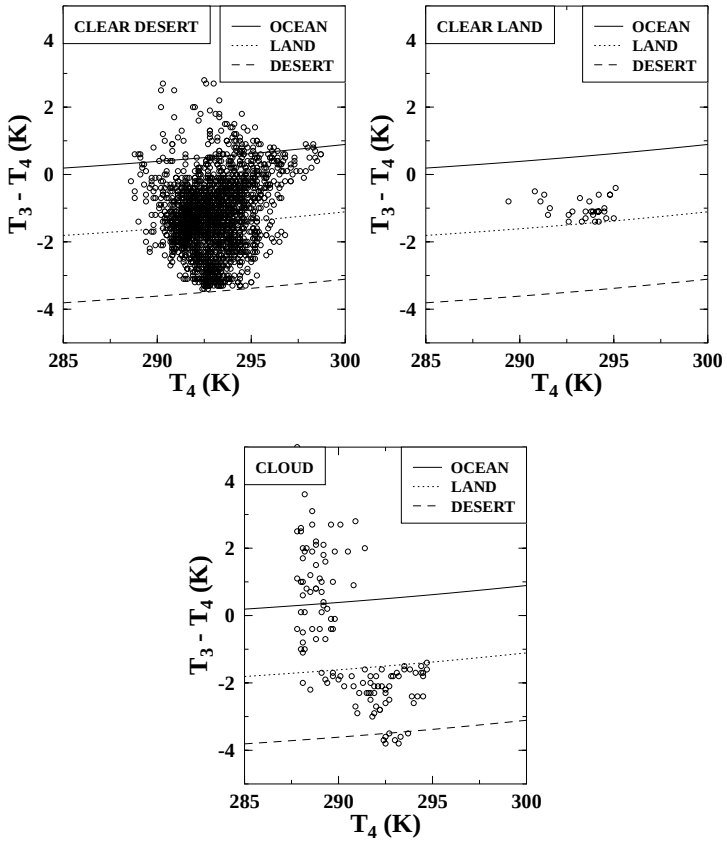

Figure 8. Scattergrams of T3-T4 (ULST) for Low Cloud and Clear Pixels Over Desert and Nondesert Land (Fig.8)

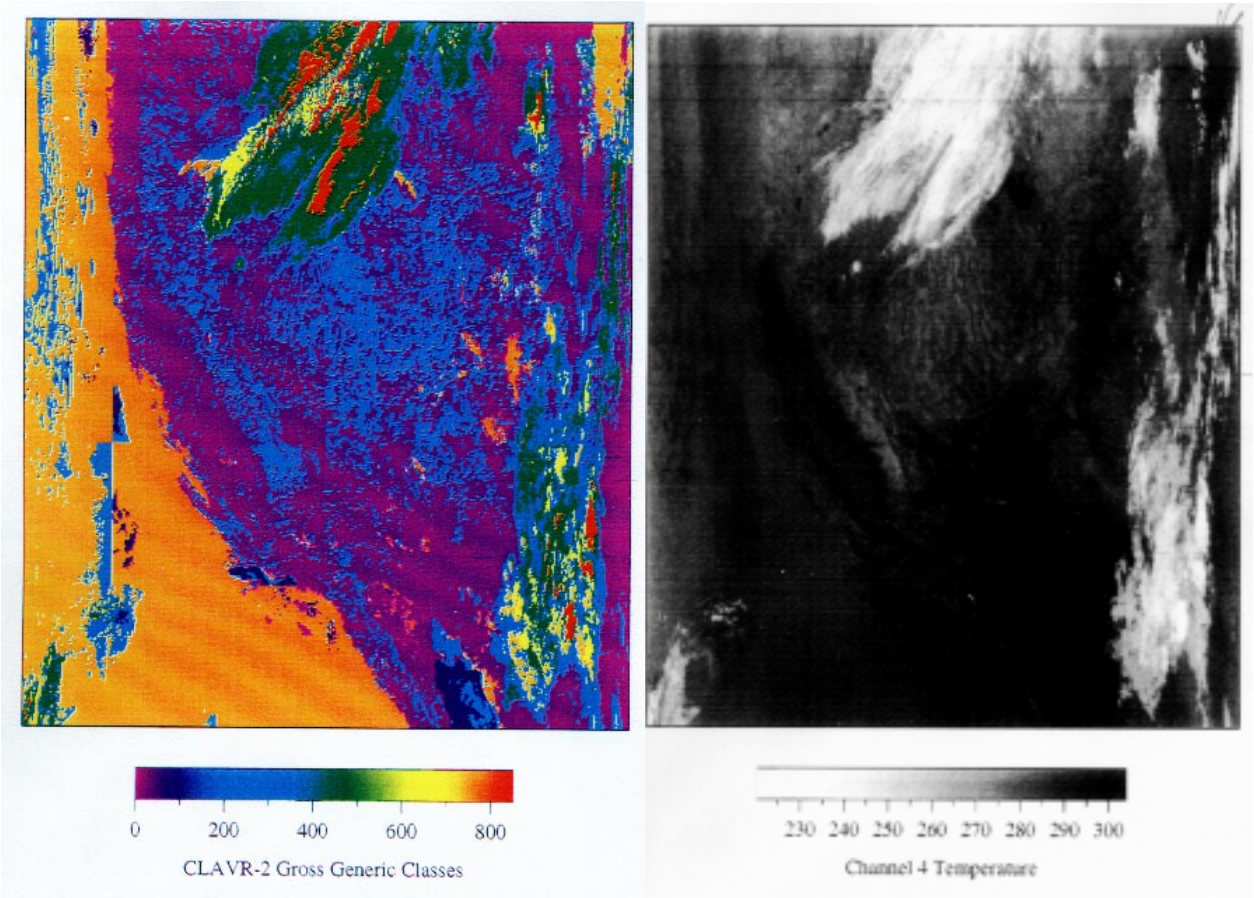

Figure 9. AVHRR GAC CH.4 Temperature and CLAVR-2 Gross Generic Cloud Classifications, Western USA and E.Pacific Coast, Orbit 489394, Nighttime, 9-6-89

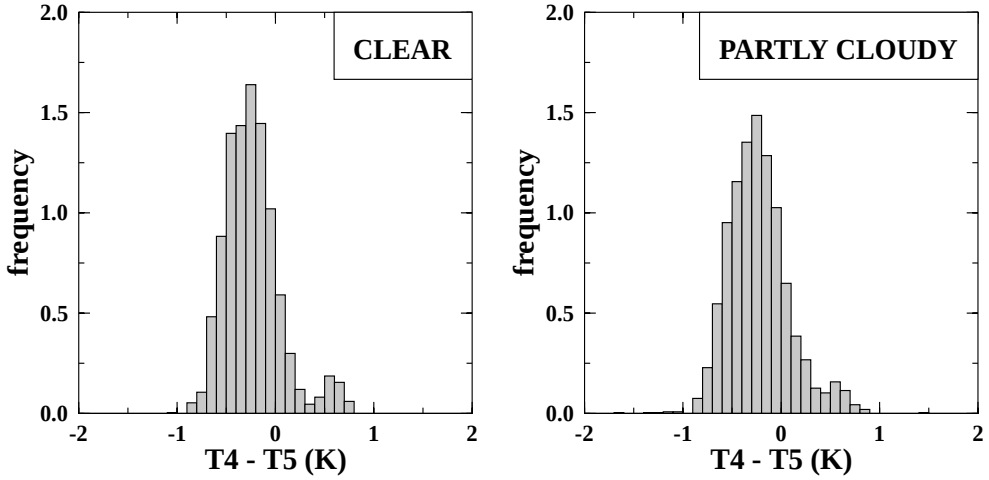

Figure 10. Nighttime Frequency Distributions of T4-T5 for Clear and Partly Cloudy Classes, Western USA, 9-6-89 (a) CLEAR T4-T5 (b) PTLY CLDY T4-T5

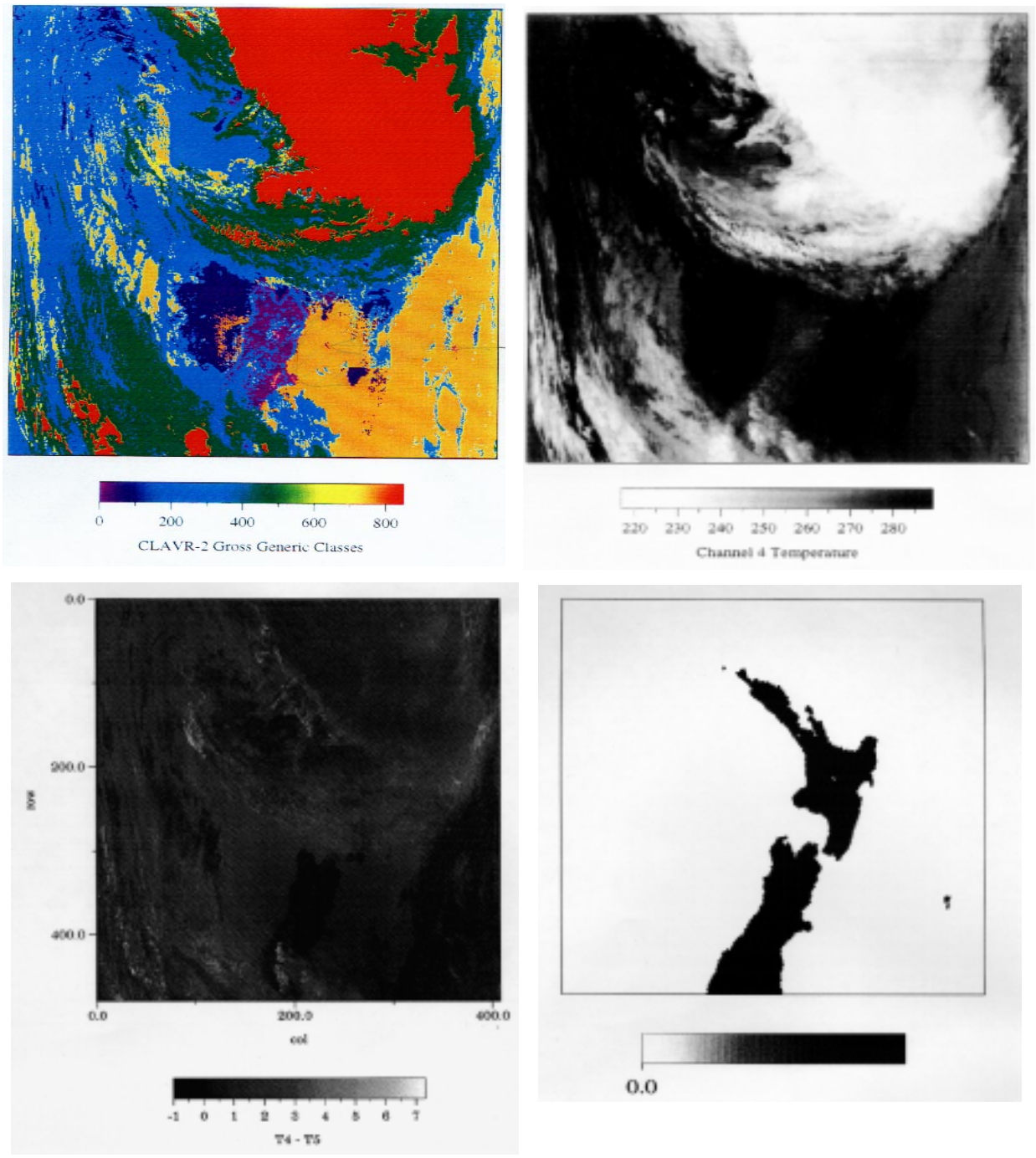

Figure 11. AVHRR GAC CH.4 Temperature and CLAVR-2 Gross Generic Cloud Classifications, New Zealand Area, Orbit 489596, Nighttime, 9-6-89